

Cloud-Scale Numerical Modeling of the Arctic  
Boundary Layer

NASA Langley Research Center Research Grant NAG-1-1718

Principal Investigator: Steven K. Krueger

Dept. of Meteorology, University of Utah  
Salt Lake City, UT 84112

*Summary of Research*

July 1, 1995–June 30, 1998

# Table of Contents

## 1. FIRE-III ACCOMPLISHMENT REPORT

## 2. FIRE-III BIBLIOGRAPHY

## 3. FIRE-III SIGNIFICANT HIGHLIGHTS

- Parameterization of Mesoscale Enhancement of Large-Scale Surface Fluxes due to Cumulus Circulations
- Two-Dimensional Numerical Simulations of Arctic Leads
- Three-Dimensional Numerical Simulations of Arctic Leads
- Simulation of a Summertime Arctic Cloudy Boundary Layer Using a 1D Turbulence Closure Model

## 4. APPENDIX: SELECTED PREPRINTS

- Parameterization of mesoscale enhancement of large-scale surface fluxes over tropical oceans
- Two-dimensional numerical simulations of Arctic leads
- Radiatively driven entrainment and turbulence in a smoke cloud
- Simulation of a summertime Arctic cloudy boundary layer using a 1D turbulence closure model

## FIRE-III ACCOMPLISHMENT REPORT

Name: Steven K. Krueger

Institution: Dept. of Meteorology, University of Utah, Salt Lake City, UT 84112

TITLE: Cloud-Scale Numerical Modeling of the Arctic Boundary Layer

### ABSTRACT:

The interactions between sea ice, open ocean, atmospheric radiation, and clouds over the Arctic Ocean exert a strong influence on global climate. Uncertainties in the formulation of interactive air-sea-ice processes in global climate models (GCMs) result in large differences between the Arctic, and global, climates simulated by different models. Arctic stratus clouds are not well-simulated by GCMs, yet exert a strong influence on the surface energy budget of the Arctic. Leads (channels of open water in sea ice) have significant impacts on the large-scale budgets during the Arctic winter, when they contribute about 50 percent of the surface fluxes over the Arctic Ocean, but cover only 1 to 2 percent of its area. Convective plumes generated by wide leads may penetrate the surface inversion and produce condensate that spreads up to 250 km downwind of the lead, and may significantly affect the longwave radiative fluxes at the surface and thereby the sea ice thickness. The effects of leads and boundary layer clouds must be accurately represented in climate models to allow possible feedbacks between them and the sea ice thickness.

The FIRE III Arctic boundary layer clouds field program, in conjunction with the SHEBA ice camp and the ARM North Slope of Alaska and Adjacent Arctic Ocean site, will offer an unprecedented opportunity to greatly improve our ability to parameterize the important effects of leads and boundary layer clouds in GCMs.

We will make extensive use of FIRE III measurements and a high-resolution numerical model, the University of Utah Cloud Resolving Model, to increase our understanding of the physical processes that determine:

- (1) the formation and structure of Arctic stratus clouds and
- (2) how leads over the Arctic Ocean affect the large-scale budgets of sensible heat, water vapor, and condensate.

This is necessary before developing lead and boundary layer cloud parameterizations based on general physical principles. We will:

- (1) Determine in detail how large-scale processes, in combination with cloud-scale radiative, microphysical, and dynamical processes, govern the formation and multi-layered structure of Arctic stratus clouds.
- (2) Quantitatively determine the effects of leads on the large-scale budgets of sensible heat, water vapor, and condensate in a variety of Arctic winter conditions.

GOALS: Our long-term research goals are to improve our ability to parameterize the important effects of Arctic leads and Arctic boundary layer clouds in GCMs.

OBJECTIVES: Our FIRE-III research objectives are:

- (1) To determine in detail how large-scale processes, in combination with cloud-scale radiative, microphysical, and dynamical processes, govern the formation and multi-layered structure of arctic stratus clouds. This information will be useful for developing and improving 1D boundary layer models for the Arctic.
- (2) To quantitatively determine the effects of leads on the large-scale budgets of sensible heat,

water vapor, and condensate in a variety of Arctic winter conditions. This information will be used to identify the most important lead-flux processes that require parameterization in climate models.

**APPROACH:** We made extensive use of a high-resolution numerical model, the 2D University of Utah Cloud Resolving Model (UU CRM), and its 1D version, the University of Utah Turbulence Closure Model (UU TCM), a boundary layer model based on third-moment turbulence closure.

#### **TASKS COMPLETED:**

- (1) Our first step toward parameterizing the effects of Arctic leads was to study the effects of cool and dry downdrafts associated with precipitating cumulus clouds on the area-averaged surface turbulent fluxes over a Tropical ocean. As over the Arctic sea ice, the local surface turbulent fluxes may vary significantly over short times and distances.
- (2) We constructed a new 3D large-eddy simulation model which will be used for studying the 3D structure of plumes generated by Arctic leads.
- (3) We ran and analyzed 2D UU CRM simulations of the 3D Glendening and Burk (1992) and 2D Alam and Curry (1994) lead-generated plume cases to gauge the impacts of model physics and dimensionality.
- (4) We used the 2D UU CRM to study how the height of plumes generated by leads in the wintertime Arctic depends on lead width, lead surface buoyancy flux, and lead orientation relative to the large-scale wind direction. We also used the 2D UU CRM to simulate the structure and impact of clouds produced by lead-generated plumes.
- (5) We ran and analyzed 1D UU TCM simulations of the McInnes and Curry (1994) Arctic stratus cloud case to investigate formation mechanisms.
- (6) We also simulated an idealized dry but radiatively driven boundary layer (one filled with radiatively active smoke) with the 1D UU TCM in order to evaluate the model by comparing the results to those from several 1D, 2D, and 3D models that participated in an intercomparison exercise.
- (7) I participated in the field phase of the FIRE-III Arctic Clouds Experiment by flying on two research flights.
- (8) We made improvements to the radiative transfer model used in the UU CRM and UU TCM:
  - (a) In order to model the effects of Arctic wintertime ice clouds on the radiative energy budget, the radiative properties of ice crystals in the infrared are needed. We developed a composite scheme that is valid for nonspherical ice particles over a wide range of size parameters.
  - (b) Because clouds alter the distribution of the solar flux between direct and diffuse components and the penetration of shortwave radiation into the sea ice depends on the ratio of diffuse to direct radiation, we have separated the direct and diffuse components of the solar flux in the radiative transfer model.
- (9) We also developed a broadband 3D radiative transfer model to study the short-wave radiative effects of the horizontally inhomogeneous Arctic stratocumulus clouds over the horizontally inhomogeneous, highly-reflective snow/ice surface.

#### **FUTURE PLANS: We will:**

- (1) Use a 3D large-eddy simulation model to study the 3D structure of lead-induced plumes.
- (2) Simulate FIRE-III and SHEBA observations of lead-generated plumes using the 2D CRM.
- (3) Develop a parameterization of the large-scale effects of leads that includes cloud production.
- (4) Use the broadband 3D radiative transfer model in combination with the 2D CRM to study the short-wave radiative effects of the horizontally inhomogeneous Arctic stratocumulus clouds over the horizontally inhomogeneous, highly-reflective snow/ice surface and the interaction of radiation and cloud dynamics.
- (5) Run and analyze 1D TCM, 2D CRM, and 3D large-eddy simulations of Arctic stratus clouds

based on FIRE-III and SHEBA measurements to evaluate and improve the models and to investigate proposed Arctic stratus cloud formation mechanisms.

(6) Run and analyze 1D TCM and 2D CRM simulations of Arctic stratus clouds based on climatological forcing and SHEBA measurements to investigate formation mechanisms and seasonal cloudiness transitions. These will include month-long (or longer) 1D TCM simulations.

(7) Coordinate the processing and assembly of integrated datasets for single-column, cloud-resolving, and large-eddy simulation models based on FIRE-III and SHEBA measurements.

(8) Incorporate the Ebert and Curry sea-ice model into the UU TCM, and the Alam and Curry lead-freezing parameterization into the UU CRM.

## RESULTS:

### SURFACE FLUXES AND CUMULUS CIRCULATIONS

The primary effect of boundary layer cumulus circulations is to increase the area-averaged wind speed over the speed of the area-averaged vector wind. By neglecting this "gustiness" effect, the area-averaged surface turbulent fluxes may be significantly underestimated. We developed a parameterization of the gustiness that relates it to the cumulus activity (Zulauf and Krueger 1997, 1998). The agreement between the gustiness simulated by the UU CRM and that observed gives us more confidence in the UU CRM's ability to predict the area-averaged effects of lead-induced convective plumes, for which few measurements currently exist.

### LEAD-GENERATED PLUMES

We verified that the dependence of the height of lead-generated plumes on lead width and lead orientation relative to the wind direction follows classical similarity solutions (for wind-parallel leads) over a wide range of lead widths, from 200 m to 6400 m, and Glendening and Burk's (1992) scaling law (for leads oriented at an angle to the wind) over a wide range of lead orientations (Zulauf and Krueger 1999).

We also found that the 2D UU CRM produces mean plume characteristics that are quite similar to those from a 3D large-eddy simulation model, and that the addition of microphysical and radiative processes has the greatest impact upon the more energetic plume circulations, such as those associated with wide leads.

### SMOKE CLOUD INTERCOMPARISON

An intercomparison of radiatively driven entrainment and turbulence in a smoke cloud (Bretherton et al. 1997) investigated an idealized case in which a convective boundary layer filled with radiatively active "smoke" is simulated by several 1D, 2D, and 3D models. We used this case to test the UU TCM. The results using the UU TCM agree well with the 3D large-eddy simulations involved in the intercomparison (Krueger et al. 1999a).

### ARCTIC STRATUS CLOUDS

We investigated the sensitivity of the formation and structure of simulated Arctic summertime boundary-layer clouds to large-scale vertical velocity and drizzle using the UU TCM (Krueger et al. 1999b). The baseline case, under conditions of no large-scale vertical motion, contains two layers of clouds: a stable fog layer near the surface and a stratus cloud in an elevated mixed layer. We found that large-scale subsidence delays the formation of the upper cloud layer, and increases the liquid water content of the fog layer. Neglecting drizzle has little impact on the cloud water mixing ratios in the upper cloud layer, but significantly increases them in the fog layer.

## FIRE-III BIBLIOGRAPHY

**Name:** Steven K. Krueger

**Address:** Dept. of Meteorology, University of Utah, Salt Lake City, UT 84112

### BIBLIOGRAPHY:

a. List of publications (including books, book chapters, and refereed papers).

- Moeng, C.-H., W.R. Cotton, C. Bretherton, A. Chlond, M. Khairoutdinov, S. Krueger, W.S. Lewellen, M.K. McVean, J.R.M. Pasquier, H.A. Rand, A.P. Siebesma, R.I. Sykes, and B. Stevens, 1996: Simulation of a stratocumulus-topped PBL: Intercomparison of different numerical codes. *Bull. Amer. Meteor. Soc.*, **77**, 216–278.
- Bechtold, P., S. K. Krueger, W. S. Lewellen, E. van Meijgaard, C.-H. Moeng, D. A. Randall, A. van Ulden, and S. Wang, 1996: Modeling a stratocumulus-topped PBL: Intercomparison among different 1D codes and with LES. *Bull. Amer. Meteor. Soc.*, **77**, 2033–2042.
- Krueger, S. K., C.-W. Su, and P. A. McMurtry, 1997: Modeling entrainment and fine-scale mixing in cumulus clouds. *J. Atmos. Sci.*, **54**, 2697–2712.
- Su, C.-W., S. K. Krueger, P. A. McMurtry, and P. H. Austin, 1998: Linear eddy modeling of droplet spectral evolution during entrainment and mixing in cumulus clouds. *Atmos. Res.*, **47–48**, 41–58.
- Bretherton, C. S., S. K. Krueger, M. C. Wyant, P. Bechtold, E. van Meijgaard, B. Stevens, and J. Teixeira, 1998: A GCS boundary layer model intercomparison study of the first ASTEX Lagrangian experiment. *Bound.-Layer Meteor.*, submitted Oct. 1997, accepted subject to major revision.
- Fu, Q., M. Cribb, H. Barker, S. K. Krueger, and A. Grossman, 1998: A study of cloud geometry effects on atmospheric solar absorption. *J. Atmos. Sci.*, submitted June 1998.
- Zulauf, M. A., and S. K. Krueger, 1998: Parameterization of mesoscale enhancement of large-scale surface fluxes over Tropical oceans. *J. Atmos. Sci.*, to be submitted Nov. 1998.

b. List of printed technical reports and non-refereed papers.

c. List of oral presentations or posters at professional society meetings and conferences.

Krueger, S. K., C.-W. Su, and P. A. McMurtry, 1995: Linear eddy modeling of entrainment and mixing in cumulus clouds. *Preprints, 1995 Conference on Cloud Physics*, Dallas, Texas, Amer. Meteor. Soc., 559–564.

Su, C.-W., S. K. Krueger, P. H. Austin, and P. A. McMurtry, 1995: Linear eddy modeling of droplet spectral evolution during turbulent mixing in cumulus clouds. *Preprints, 1995 Conference on Cloud Physics*, Dallas, Texas, Amer. Meteor. Soc., 565–568.

Krueger, S. K., and P. A. McMurtry, 1995: Dynamic linear eddy modeling of convective boundary layers. *Preprints, 11th Symposium on Boundary Layers and Turbulence*, Charlotte, N. C., Amer. Meteor. Soc., 63–66.

Krueger, S. K., 1995: The stratus to cumulus transition in the subtropical marine boundary layer. *Preprints, 11th Symposium on Boundary Layers and Turbulence*, Charlotte, N. C., Amer. Meteor. Soc., 224–227.

Krueger, S. K., and C.-H. Chen, 1995: Testing a boundary layer cloud parameterization using CEM results. *Proceedings, Workshop on Microphysics in GCMs*, Kananaskis, Alberta, Canada, WCRP, (in press).

Krueger, S. K., 1995: Intercomparison of model results for the ASTEX Lagrangian experiments. *2d GCSS Workshop on Boundary Layer Clouds*, KNMI, De Bilt, The Netherlands, 30 August–1 September 1995.

Krueger, S. K., and C. S. Bretherton, 1995: ASTEX Lagrangian simulations. *Cloud Modeling and Measurement Workshop*, NOAA/ETL, Boulder, CO, 23–25 October 1995.

Krueger, S. K., C.-H. Chen, M. C. Wyant, and C. S. Bretherton, 1996: Simulations of the ASTEX Lagrangian experiments with 1D and 2D boundary layer models. *Proceedings, 12th International Conference on Clouds and Precipitation*, Zurich, Switzerland, 709–713.

Su, C.-W., S. K. Krueger, P. A. McMurtry, and P. H. Austin, 1996: Linear eddy modeling of droplet spectral evolution during entrainment and mixing in cumulus clouds. *Proceedings, 12th International Conference on Clouds and Precipitation*, Zurich, Switzerland, 41–44.

- Barker, H.W., L.H. Chambers, B. Stevens, and S.K. Krueger, 1996: Parameterizing sub-grid scale radiative properties of oceanic boundary layer clouds in atmospheric circulation models. *Abstracts, International Radiation Symposium*, Fairbanks, Alaska, 37.
- Krueger, S. K., 1996: GCSS: GEWEX Cloud System Study. ARM Science Team Meeting, San Antonio, TX, 4-7 March 1996.
- Krueger, S. K., 1996: Modeling stratocumulus clouds. 4th International WMO Cloud Modeling Workshop, Clermont-Ferrand, France, 12-16 August 1996.
- Krueger, S. K., 1996: Simulations of the ASTEX Lagrangian experiments with a 2D boundary layer model. 3rd GCSS Boundary Layer Cloud Workshop, Clermont-Ferrand, France, 13-16 August 1996.
- Zulauf, M., and S. K. Krueger, 1997: Parameterization of mesoscale enhancement of large-scale surface fluxes over tropical oceans. *Preprints, 22nd Conference on Hurricanes and Tropical Meteorology*, Fort Collins, CO, Amer. Meteor. Soc., 164-165.
- Krueger, S. K., and M. Zulauf, 1997: Parameterization of mesoscale enhancement of large-scale surface fluxes over tropical oceans. *Preprints, 12th Symposium on Boundary Layers and Turbulence*, Vancouver, B.C., Canada, Amer. Meteor. Soc., 494-495.
- Fu, Q., Cribb, M., Barker, H. W., and Krueger, S. K., 1998: A study of atmospheric absorption of solar radiation using cloud fields derived from a cloud resolving model. *Proceedings of the Eighth Atmospheric Radiation Measurement (ARM) Science Team Meeting*, Tucson, Arizona, DOE, (in press).
- Zulauf, M. A., and S. K. Krueger, 1999: Two-dimensional numerical simulations of Arctic leads. *Preprints, Fifth Conference on Polar Meteorology and Oceanography*, Dallas, TX, Amer. Meteor. Soc., (in press).
- Krueger, S. K., S. Liu, and Q. Fu, 1999: Simulation of a summertime Arctic cloudy boundary layer using a 1D turbulence closure model. *Preprints, Fifth Conference on Polar Meteorology and Oceanography*, Dallas, TX, Amer. Meteor. Soc., (in press).
- Krueger, S. K., S. Liu, and Q. Fu, 1999: Radiatively driven entrainment and turbulence in a smoke cloud. *Preprints, 13th Symposium on Boundary Layers and Turbulence*, Dallas, TX, Amer. Meteor. Soc., (in press).

## FIRE-III SIGNIFICANT HIGHLIGHTS

Name: Steven K. Krueger

Address: Dept. of Meteorology, University of Utah, Salt Lake City, UT 84112

### SIGNIFICANT HIGHLIGHT: Parameterization of Mesoscale Enhancement of Large-Scale Surface Fluxes due to Cumulus Circulations

Large-scale models typically diagnose the surface turbulent fluxes of sensible and latent heat using the large-scale (i.e., area-averaged) near-surface temperature and water vapor mixing ratio and the speed of the large-scale wind vector. These fluxes may be called the "vector-mean" surface fluxes. Esbensen and McPhaden (1996) defined "mesoscale enhancement" as the difference between the vector-mean surface fluxes and the actual large-scale surface fluxes. In the absence of mesoscale circulations, there would be no mesoscale enhancement.

Based on TOGA TAO buoy data, Esbensen and McPhaden found that mesoscale enhancement of evaporation can reach 30% of the total evaporation. They also showed that mesoscale enhancement is primarily due to mesoscale wind variability ("gustiness") and is associated with periods of significant precipitation.

Multi-day, large-domain simulations of tropical convection performed with the 2D University of Utah Cloud Resolving Model indicate that the characteristics of mesoscale enhancement as simulated by the model are quite similar to those observed.

In the accompanying figure, the blue lines show the time series of the simulated large-scale surface wind speed (top panel) and latent heat flux (bottom panel). The green lines show the speed of the simulated large-scale wind vector (top) and the latent heat flux calculated using this speed (bottom). Mesoscale enhancement is the difference between the blue and green lines in the bottom panel.

If the large-scale surface wind speed (blue line, top) is used in place of the speed of the large-scale wind vector (green line, top) to calculate the surface fluxes, the resulting fluxes are practically identical to the actual fluxes (blue line, bottom). Observations support this conclusion, as well.

We have developed a parameterization of the large-scale surface wind speed. It augments the speed of the large-scale wind vector with a gustiness speed that is directly linked to a measure of cumulus activity, (the updraft cumulus mass flux at cloud base level, which is available in many global climate models). The red lines in the figure show the large-scale surface wind speed estimated using the parameterization (top) and the latent heat flux calculated using this speed (bottom). The good agreement between the red and blue lines indicates that the parameterization of mesoscale enhancement is successful.

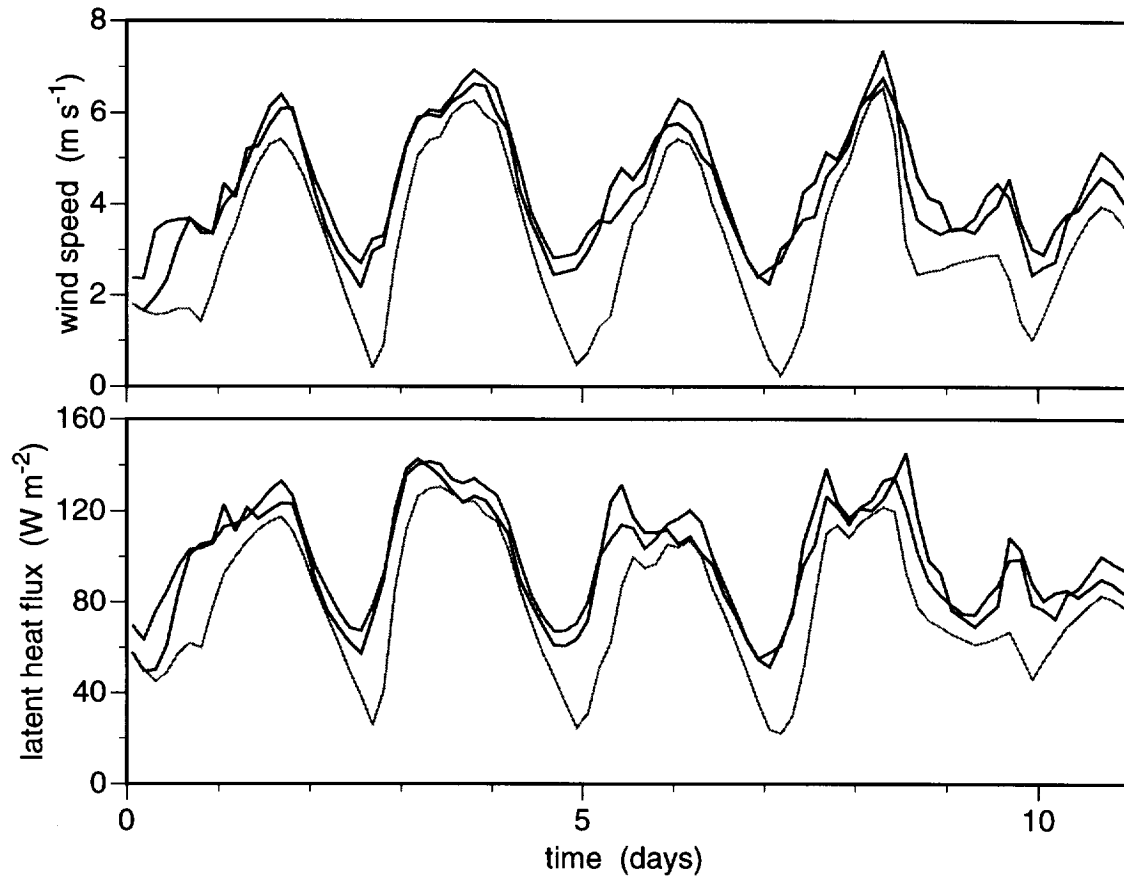


Figure 1: *Blue lines*: simulated large-scale surface wind speed (top) and latent heat flux (bottom). *Green lines*: speed of the large-scale wind vector (top) and the latent heat flux calculated using this speed (bottom). *Red lines*: estimated large-scale surface wind speed based on a parameterization that links gustiness to cumulus activity (top) and the latent heat flux calculated using this speed (bottom).

## FIRE-III SIGNIFICANT HIGHLIGHTS

Name: Steven K. Krueger

Address: Dept. of Meteorology, University of Utah, Salt Lake City, UT 84112

### SIGNIFICANT HIGHLIGHT: Two-Dimensional Numerical Simulations of Arctic Leads

Leads (channels of open water in sea ice) have significant impacts on the large-scale budgets during the Arctic winter, when they contribute about 50 percent of the surface fluxes over the Arctic Ocean, but cover only 1 to 2 percent of its area. Convective plumes generated by wide leads may penetrate the surface inversion and produce condensate that spreads up to 250 km downwind of the lead, and may significantly affect the longwave radiative fluxes at the surface and thereby the sea ice thickness. The effects of leads must be accurately represented in climate models to allow possible feedbacks between them and the sea ice thickness.

We used a high-resolution numerical model, the University of Utah Cloud Resolving Model (UU CRM), to increase our understanding of the physical processes that determine how leads over the Arctic Ocean affect the large-scale budgets of sensible heat, water vapor, and condensate. This is necessary before developing lead parameterizations based on general physical principles. During FIRE-III:

- We ran and analyzed 2D UU CRM simulations of the 3D Glendening and Burk (1992) and 2D Alam and Curry (1994) lead-generated plume cases to gauge the impacts of model physics and dimensionality.

We found that the 2D UU CRM produces mean plume characteristics that are quite similar to those from a 3D large-eddy simulation model, and that the addition of microphysical and radiative processes has the greatest impact upon the more energetic plume circulations, such as those associated with wide leads.

- We used the 2D UU CRM to study how the height of plumes generated by leads in the wintertime Arctic depends on lead width, lead surface buoyancy flux, and lead orientation relative to the large-scale wind direction.

We verified that the dependence of the height of lead-generated plumes on lead width follows classical similarity solutions (for wind-parallel leads) over a wide range of lead widths, from 200 m to 6400 m, (see top panel of figure), and that the dependence on lead orientation relative to the wind direction follows Glendening and Burk's (1992) scaling law (for leads oriented at an angle to the wind) over a wide range of lead orientations (Zulauf and Krueger 1999) (see bottom panel of figure).

These results not only indicate that the 2D UU CRM will be a useful for determining how leads over the Arctic Ocean affect the large-scale budgets of sensible heat, water vapor, and condensate, but that knowledge of the lead width and orientation distributions are needed in order to parameterize the effects of leads on the atmosphere and on the surface heat budget.

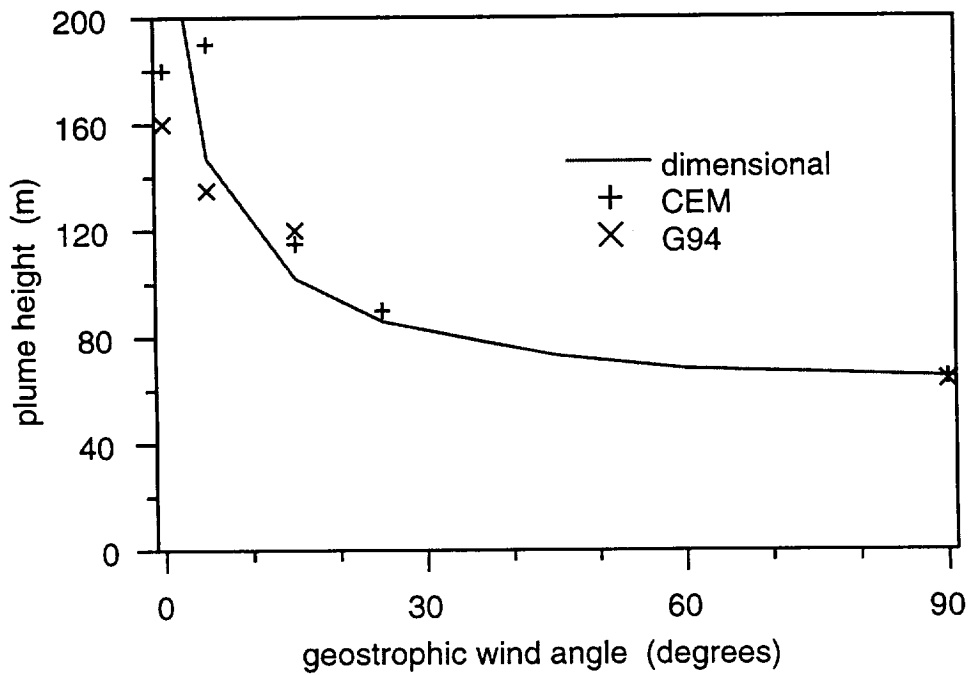
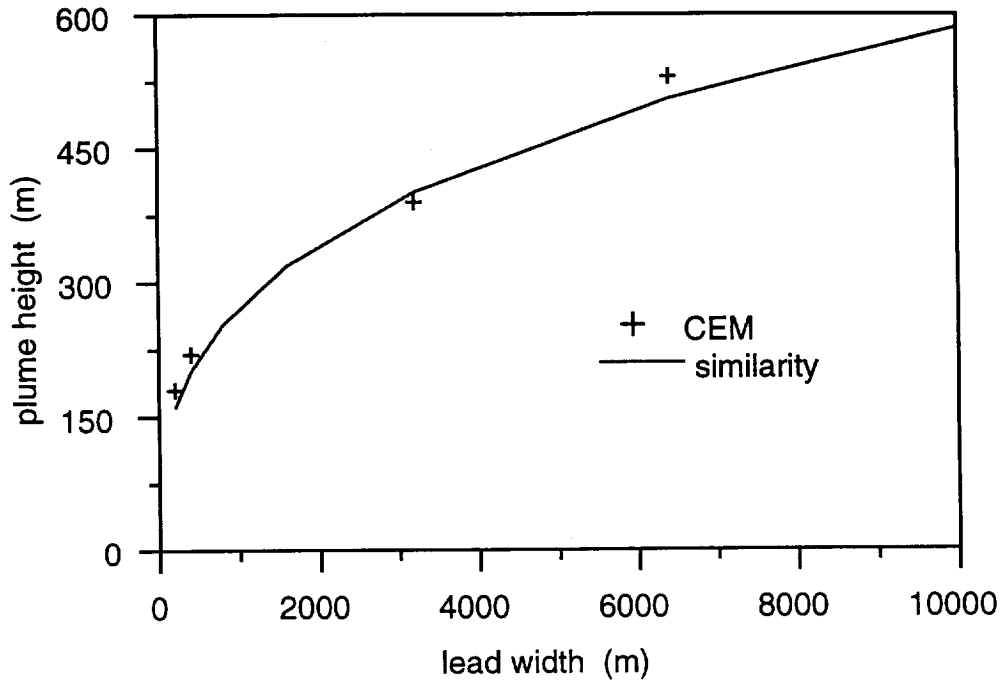


Figure 1: Comparison of simulation derived plume heights with theoretical solutions for cases with specified surface fluxes and no geostrophic cross-wind (top), and those with diagnosed surface fluxes and geostrophic cross-wind (bottom).

## FIRE-III SIGNIFICANT HIGHLIGHTS

Name: Steven K. Krueger

Address: Dept. of Meteorology, University of Utah, Salt Lake City, UT 84112

### SIGNIFICANT HIGHLIGHT: Three-Dimensional Numerical Simulations of Arctic Leads

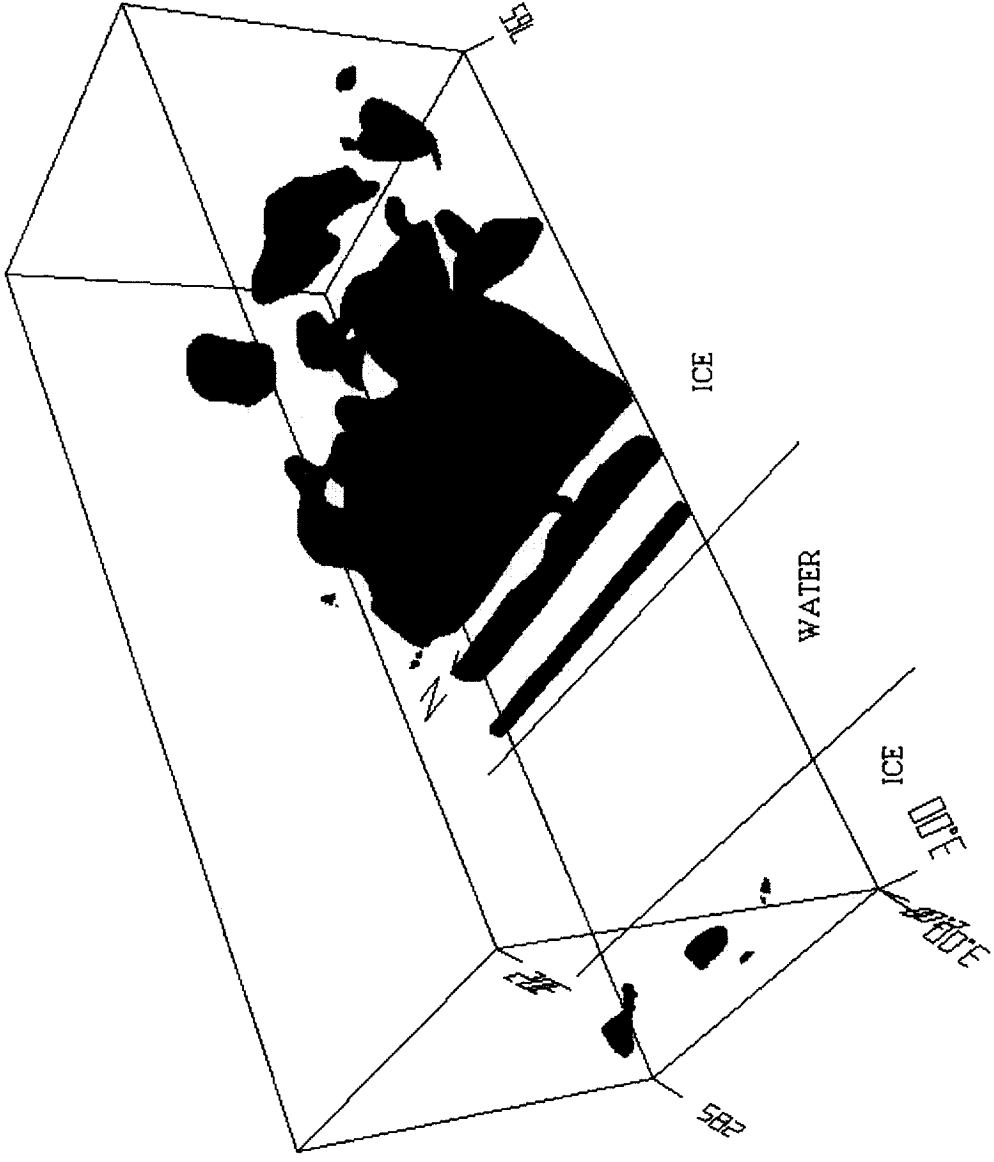
Leads (channels of open water in sea ice) have significant impacts on the large-scale budgets during the Arctic winter, when they contribute about 50 percent of the surface fluxes over the Arctic Ocean, but cover only 1 to 2 percent of its area. Convective plumes generated by wide leads may penetrate the surface inversion and produce condensate that spreads up to 250 km downwind of the lead, and may significantly affect the longwave radiative fluxes at the surface and thereby the sea ice thickness. The effects of leads must be accurately represented in climate models to allow possible feedbacks between them and the sea ice thickness.

We used a high-resolution numerical model, the University of Utah Cloud Resolving Model (UU CRM), to increase our understanding of the physical processes that determine how leads over the Arctic Ocean affect the large-scale budgets of sensible heat, water vapor, and condensate. This is necessary before developing leadparameterizations based on general physical principles.

During FIRE-III:

- We ran and analyzed 2D UU CRM simulations of the 3D Glendening and Burk (1992) and 2D Alam and Curry (1994) lead-generated plume cases to gauge the impacts of model physics and dimensionality.
- We used the 2D UU CRM to study how the height of plumes generated by leads in the wintertime Arctic depends on lead width, lead surface buoyancy flux, and lead orientation relative to the large-scale wind direction. We also used the 2D UU CRM to simulate the structure and impact of clouds produced by lead-generated plumes.
- We constructed a new 3D large-eddy simulation model which will be used for studying the 3D structure of plumes generated by Arctic leads. In particular, we will use it to evaluate the 2D UU CRM simulations.

The figure shows a snapshot from a 3D large-eddy simulation of a lead-generated convective plume using our new model. The 20 cm/s vertical velocity iso-surface is displayed. On the scale of the lead width, the plume's updraft structure is essentially two-dimensional. However, on smaller scales many 3D turbulent eddies are evident. These eddies are responsible for most of the vertical transport of heat and water vapor, so their effects must be accurately represented in the 2D CRM.



Snapshot from a University of Utah 3D large-eddy simulation of a lead-generated convective plume. The 20 cm/s vertical velocity iso-surface is displayed. The air temperature is  $-27^{\circ}\text{C}$ , the ice temperature is  $-29^{\circ}\text{C}$ , and the water temperatures is  $-2^{\circ}\text{C}$ .

## FIRE-III SIGNIFICANT HIGHLIGHTS

Name: Steven K. Krueger

Address: Dept. of Meteorology, University of Utah, Salt Lake City, UT 84112

**SIGNIFICANT HIGHLIGHT:** Simulation of a Summertime Arctic Cloudy Boundary Layer Using a 1D Turbulence Closure Model

Arctic stratus clouds (ASC) significantly affect the surface energy budget of the Arctic, and thereby the sea ice thickness. The formation mechanism(s) of these clouds are still uncertain. ASC often occur in multiple layers. The lowest layer may rest on the surface. The upper cloud layer or layers are decoupled from the stable surface layer, thus their source of water vapor does not appear to be the surface.

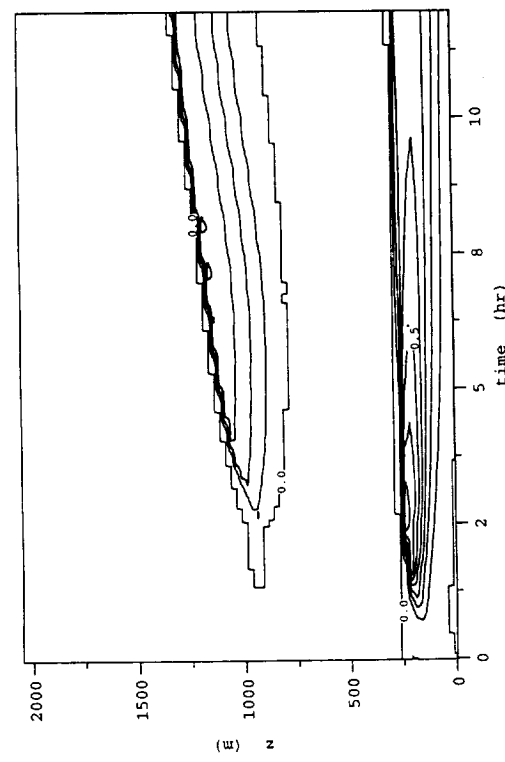
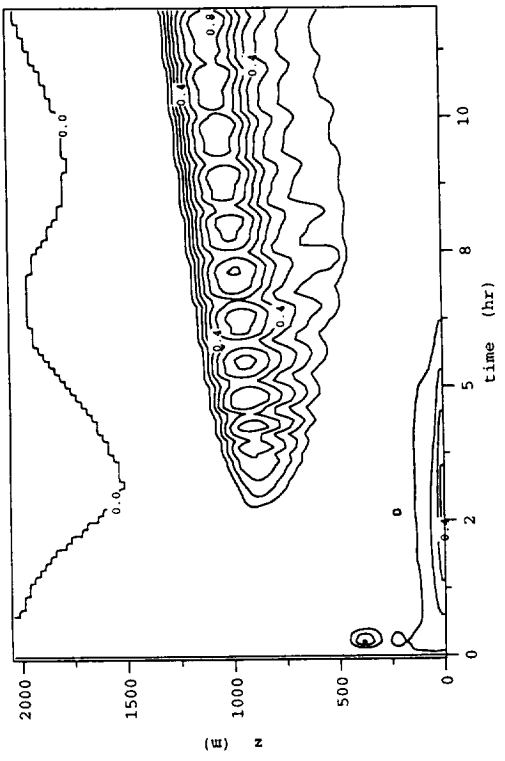
Several layering mechanisms have been proposed:

- Herman and Goody (1976): Solar absorption warms the interior of a surface-based cloud and thereby forms a clear layer between two cloudy layers.
- Tsay and Jayaweera (1984): The upper cloud layer is formed by very weak ascent or entrainment, while the surface cloud layer is an advective fog.
- McInnes and Curry (1995): The upper cloud layer is maintained by cloud-top radiative cooling, while the lower cloud layer is formed by radiative cooling at the base of the upper mixed layer.

1D second-moment turbulence closure models have reproduced many aspects of the structure of the summertime Arctic boundary layer. We used the University of Utah 1D third-moment turbulence closure model (which includes a simple drizzle parameterization and an interactive radiative transfer scheme) to simulate an Arctic summertime boundary layer based on observations obtained on June 28, 1980, during the Arctic Stratus Experiment (McInnes and Curry 1995).

The figure shows time-height plots of cloud water mixing ratio and turbulent kinetic energy from a simulation with no drizzle and no large-scale vertical motion. (Including drizzle makes little difference.) There are two cloud layers: a stable fog layer near the surface and a stratus cloud in an elevated turbulently mixed layer. The upper cloud layer slowly ascends due to entrainment. Both layers form due to cloud-top radiative cooling; the fog layer is also cooled by contact with the surface.

The ability of this model to simulate the formation and structure of a summertime Arctic cloudy boundary layer suggests that it should be useful for studies of boundary layers observed during the FIRE-III Arctic Cloud Experiment.



Time-height plots of cloud water mixing ratio ( $\text{g kg}^{-1}$ ) (left) and turbulent kinetic energy ( $\text{m}^2 \text{s}^{-2}$ ) (right) from a simulation of an Arctic summertime boundary layer using the University of Utah 1D turbulence closure model. The simulation is based on observations obtained on June 28, 1980, during the Arctic Stratus Experiment.

## APPENDIX: SELECTED PREPRINTS

- Krueger, S. K., and M. Zulauf, 1997: Parameterization of mesoscale enhancement of large-scale surface fluxes over tropical oceans. *Preprints, 12th Symposium on Boundary Layers and Turbulence*, Vancouver, B.C., Canada, Amer. Meteor. Soc., 494–495.
- Zulauf, M. A., and S. K. Krueger, 1999: Two-dimensional numerical simulations of Arctic leads. *Preprints, Fifth Conference on Polar Meteorology and Oceanography*, Dallas, TX, Amer. Meteor. Soc., (in press).
- Krueger, S. K., S. Liu, and Q. Fu, 1999: Radiatively driven entrainment and turbulence in a smoke cloud. *Preprints, 13th Symposium on Boundary Layers and Turbulence*, Dallas, TX, Amer. Meteor. Soc., (in press).
- Krueger, S. K., S. Liu, and Q. Fu, 1999: Simulation of a summertime Arctic cloudy boundary layer using a 1D turbulence closure model. *Preprints, Fifth Conference on Polar Meteorology and Oceanography*, Dallas, TX, Amer. Meteor. Soc., (in press).

Steven K. Krueger\* and Michael Zulauf  
 University of Utah, Salt Lake City, Utah

## 1. INTRODUCTION

Large-scale models typically diagnose the surface turbulent fluxes of sensible and latent heat over the ocean using the large-scale (i.e., area-averaged) near-surface temperature and water vapor mixing ratio and the speed of the large-scale wind vector. These fluxes may be called the “vector-mean” surface fluxes. Esbensen and McPhaden (1996) defined “mesoscale enhancement” as the difference between the vector-mean surface fluxes and the actual large-scale surface fluxes. In the absence of mesoscale circulations, there would be no mesoscale enhancement.

Based on TOGA TAO buoy data, Esbensen and McPhaden found that mesoscale enhancement of evaporation can reach 30% of the total evaporation. They also showed that mesoscale enhancement is primarily due to mesoscale wind variability (“gustiness”) and is associated with periods of significant precipitation.

Analyses of two multi-day, large-domain simulations of tropical maritime convection performed with the 2D UCLA cumulus ensemble model (CEM) indicate that the characteristics of mesoscale enhancement as simulated by the model are quite similar to those observed. Xu et al. (1992) describe the two simulations (Q02 and Q03) in detail. Each simulation was for 11 days in a 512-km domain with a horizontal grid size of 2 km.

## 2. SURFACE FLUX CALCULATIONS

In the CEM, the bulk aerodynamic method of Deardorff (1972) is used to calculate the local (i.e., gridpoint) latent and sensible heat fluxes at the surface,  $E$  and  $S$ . Using the notation of Esbensen and McPhaden, the domain-averaged latent heat flux,  $\langle E \rangle$ , for example, is then

$$\langle E \rangle = \rho L_v \langle C_q(U, \cdot) U (q_s - q) \rangle,$$

where  $\rho$  is the density,  $L_v$  is the latent heat of vaporization,  $C_q$  is the stability-dependent transfer coefficient,  $U$  is the wind speed,  $q_s$  is the surface mixing ratio,  $q$  is the near-surface mixing ratio, and angle brackets indicate the domain average. The corresponding vector-mean flux is

$$E_v = \rho L_v C_q(V, \cdot) V (\langle q_{sfc} \rangle - \langle q \rangle),$$

where  $V$  is the magnitude of the average (or resultant) wind vector, which is predicted by large-scale models.

\* Corresponding author address: Department of Meteorology, University of Utah, Salt Lake City, UT 84112. E-mail: krueger@ucar.edu

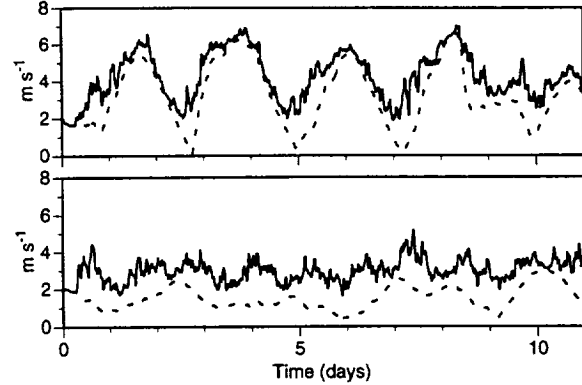


Figure 1. For Q02 (top) and Q03 (bottom):  $\langle U \rangle$  (solid) and  $V$  (dashed).

By replacing  $V$  with the domain-averaged wind speed,  $\langle U \rangle$ , we obtain the scalar-mean flux,

$$E_s = \rho L_v C_q(\langle U \rangle, \cdot) \langle U \rangle (\langle q_s \rangle - \langle q \rangle).$$

As can be seen in Fig. 1, the differences between  $\langle U \rangle$  and  $V$  can be significant. Fig. 2 compares the vector-mean and scalar-mean latent heat fluxes with the domain-averaged flux. The results are similar for the corresponding sensible heat fluxes. We see that mesoscale enhancement is significant, and that the vector-mean flux does a poor job of estimating the averaged flux, while the scalar-mean flux tracks it extremely well. Table 1 summarizes these results.

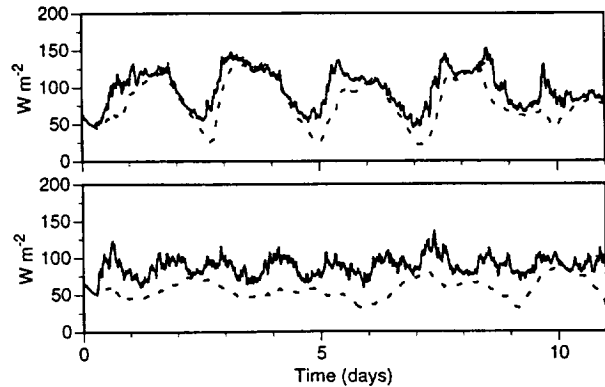


Figure 2. For Q02 (top) and Q03 (bottom):  $\langle E \rangle$  (solid),  $E_v$  (dashed), and  $E_s$  (dotted).

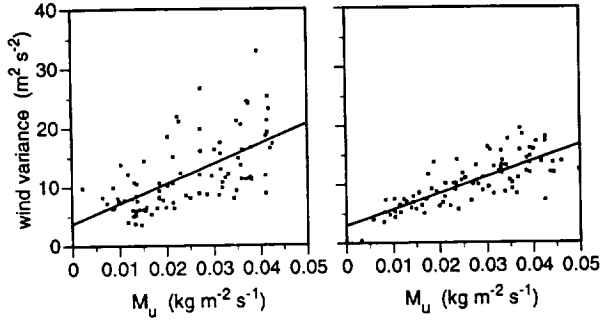


Figure 3. For Q02 (left) and Q03 (right): scatter plots of  $M_u$  at  $z=566$  m vs.  $U_\sigma^2$ .

### 3. WIND SPEED PARAMETERIZATION

We can approximate the scalar-mean fluxes, which are good estimates of the large-scale (i.e., domain-averaged) fluxes, if we can parameterize  $\langle U \rangle$  in terms of  $V$ . Since  $V$  is always less than or equal to  $\langle U \rangle$ , we may introduce a gustiness speed,  $U_g$ , such that

$$\langle U \rangle^2 = V^2 + U_g^2. \quad (1)$$

The variance of the horizontal wind speed,

$$U_\sigma^2 \equiv \langle u'^2 \rangle + \langle v'^2 \rangle,$$

where  $u'$  and  $v'$  are the local deviations from  $\langle u \rangle$  and  $\langle v \rangle$ , the components of the average wind vector, can be formally related to the gustiness speed:

$$U_g = \alpha U_\sigma. \quad (2)$$

Theoretical methods give a value of 0.8 for  $\alpha$  (Jabouille et al. 1996). In our simulations,  $\alpha$  is usually between 0.75 and 0.85. These results suggest that a constant value of  $\alpha$  is a good approximation. Then  $U_g$ , and hence  $\langle U \rangle$ , may be obtained if  $U_\sigma$  can be parameterized.

We will assume that the wind speed variance is primarily due to mesoscale circulations driven by cumulus convection. If this is the case,  $U_\sigma^2$  should be related to a measure of the intensity of the cumulus convection, such as the updraft cloud mass flux,  $M_u$ . Typical relationships between the two are shown in Fig. 3, where 3-hour averages of  $M_u$  at cloud-base level and  $U_\sigma^2$  from Q02 and Q03 are related through scatterplots. In each instance, a least squares fit to a line was performed. The fit for Q02 has a correlation coefficient of 0.39, while that for Q03 is substantially better, with a correlation coefficient of 0.61. The differences reflect differences in the mesoscale organization of convection between Q02 and Q03.

The linear fits displayed in Fig. 3 form the basis of a parameterization of  $\langle U \rangle$  that augments  $V$  with a gustiness speed that is linked via  $U_\sigma^2$  to a measure of cumulus activity,  $M_u$  at cloud-base level, which is available in many large-scale models.

Table 1 lists the time-average and rms errors for large-scale fluxes obtained using various parameterization methods. The first line of each part of the table

Table 1. Time-averages and rms errors ( $W/m^2$ ) for large-scale fluxes from various parameterizations.

Case	Method	rms		rms	
		$\langle [E] \rangle$	$\langle E \rangle$	$\langle [S] \rangle$	$\langle S \rangle$
Q02	$\langle E \rangle, \langle S \rangle$	99.5	0.0	17.4	0.0
	$E_v, S_v$	80.4	24.8	13.7	5.2
	$E_s, S_s$	100.4	2.0	17.4	0.8
	$U_g \leftarrow U_\sigma$	101.0	3.7	17.5	0.9
	$U_g \leftarrow [U_g]$	98.1	9.7	16.9	2.3
	$U_\sigma^2 \leftarrow M_u$	100.8	7.9	17.4	1.7
Q03	$\langle E \rangle, \langle S \rangle$	88.2	0.0	17.5	0.0
	$E_v, S_v$	57.4	33.4	11.1	6.9
	$E_s, S_s$	90.5	2.4	17.7	0.4
	$U_g \leftarrow U_\sigma$	91.0	3.5	17.8	0.6
	$U_g \leftarrow [U_g]$	89.6	8.6	17.5	1.7
	$U_\sigma^2 \leftarrow M_u$	90.7	6.4	17.7	1.2

shows the actual domain-averaged fluxes, time-averaged over the last 10.5 days of the 11-day runs. The second line shows the vector-mean fluxes, and the third line the scalar-mean fluxes. The fourth line shows an approximation of the scalar-mean fluxes obtained using (1) and (2) with a constant value for  $\alpha$  (the theoretical value of 0.8) along with the actual  $U_\sigma$ .

The fifth line of each table presents approximate scalar-mean fluxes obtained using (1) and the time average of  $U_g$  ( $2.5 \text{ m s}^{-1}$  in both runs). For both Q02 and Q03, this method recovers the mean values of the fluxes rather well, but the lack of any time variation in the gustiness leads to large rms errors. Finally, the sixth line shows the approximate scalar-mean fluxes obtained using (1), (2), and the parameterization for wind speed variance in terms of updraft cloud mass flux shown in Fig. 3. The rms errors are less than those for the average  $U_g$  method, while the mean errors are similar to those for the actual scalar-mean fluxes.

ACKNOWLEDGMENTS. This research was supported by NASA Grant NAG 1-1718.

### REFERENCES

- Deardorff, J. W., 1972: Parameterization of the planetary boundary layer for use in general circulation models. *Mon. Wea. Rev.*, **100**, 93–106.
- Esbensen, S. K., and M. J. McPhaden, 1996: Enhancement of tropical ocean evaporation and sensible heat flux by atmospheric mesoscale systems. *J. Clim.*, **9**, 2307–2325.
- Jabouille, P., J. L. Redelsperger, and J. P. Lafore, 1996: Modification of surface fluxes by atmospheric convection in the TOGA-COARE region. *Mon. Wea. Rev.*, **124**, 816–837.
- Xu, K.-M., A. Arakawa, and S. K. Krueger, 1992: The macroscopic behavior of cumulus ensembles simulated by a cumulus ensemble model. *J. Atmos. Sci.*, **49**, 2402–2420.

Michael A. Zulauf \* and Steven K. Krueger  
University of Utah, Salt Lake City, Utah

## 1. INTRODUCTION

Arctic leads, due to the extreme temperature differences between the sea surface and the winter atmosphere, can be a significant source of moisture and heat for the polar atmosphere. Because of their relatively small scales however, these openings in the pack ice cannot be explicitly resolved by large-scale models.

Previous studies have examined some of the various factors which influence the convective plumes that develop in the vicinity of leads. Glendening and Burk (1992) and Glendening (1994), hereafter referred to as GB92 and G94 respectively, examined the impact of orientation of the large-scale wind field over a 200 m wide lead. GB92 and G94 also evaluated the heat transport budget extensively. They conducted three-dimensional large-eddy simulations (LES), wherein the model had been modified to handle the stable stratification of the Arctic winter atmosphere. Alam and Curry (1995, hereafter AC95) used a two-dimensional model to investigate the impacts of lead width and large scale wind field upon plume evolution.

In the present study, the two-dimensional cloud resolving model (CRM) of Krueger, McLean, and Fu (1995) is employed to attempt to verify, and build upon the previous findings. The sensitivity to ambient wind speed and orientation, and lead width is investigated. Comparisons are made with the previous LES and two-dimensional studies, and with results obtained from similarity and dimensional theory. For the most part, previous studies have not included physical processes such as latent heating, liquid/ice microphysics, and radiation. The CRM can be used to help gauge the relative importance of these processes.

By examining the atmospheric circulations created by the leads, we hope to obtain a better understanding of the impact the enhanced small-scale surface fluxes can have upon the large-scale. This will help facilitate an improved understanding of how Arctic leads influence the Arctic climate.

## 2. SIMULATION PARAMETERS

The model parameters are essentially the same as those employed by GB92 and G94. The atmospheric

\* Corresponding author address: Michael A. Zulauf  
Department of Meteorology, University of Utah, Salt Lake City,  
UT 84112. e-mail: mazulauf@atmos.met.utah.edu

base state is stably stratified with potential temperature increasing at  $10 \text{ K km}^{-1}$ , from a surface air temperature of  $-27^\circ\text{C}$ . The ice and water surface temperatures are  $-29^\circ\text{C}$  and  $-2^\circ\text{C}$ , respectively. The large-scale geostrophic wind is fixed at  $2.5 \text{ m s}^{-1}$ , while its direction with respect to the lead varies depending upon the simulation. Surface roughness values of 0.1 and 0.01 cm are used for the ice and water, respectively. The Coriolis parameter is calculated at a latitude of  $79^\circ\text{N}$ . Unless otherwise noted, all simulations neglect microphysical and radiative processes.

In the experiments presented herein, the horizontal domains range over more than two orders of magnitude. The vertical domains vary to a lesser extent than the horizontal, and are typically deep enough to ensure that wave reflection off of the model top is not a significant problem. The grid spacing and time step vary depending upon the simulation. The lead-perpendicular boundaries are periodic, and the top boundary allows no penetration. To better quantify turbulent and time varying flow fields, all results are time averaged over a specified period near the end of each simulation. Run times span a range from approximately 12 minutes to 6 hours.

## 3. EFFECTS OF VARYING WIND ORIENTATION

As stated in G94, plume development depends strongly upon transit time of an air parcel across the lead. When the time period is less than the Brunt Väisälä period  $P$ , maximum plume development will occur downstream of the lead. When the transit time is greater than the Brunt Väisälä period, maximum plume development occurs over the lead.

Fig. 1 compares the vertical turbulent temperature flux obtained by GB92 and the present study, for a 200 m wide lead with the geostrophic wind oriented at a  $90^\circ$  angle to the lead. Note that, as is the case with many of the figures presented, only a portion of the computational domain is displayed. For this case the transit time is approximately  $P/4$ , which is not enough time for a well developed and distinct plume to form over the lead. While the shape of the LES and CRM plumes differ substantially, the magnitude of the fluxes and the depth of penetration show excellent agreement. For both simulations the plume penetrates to a depth of about 65 m.

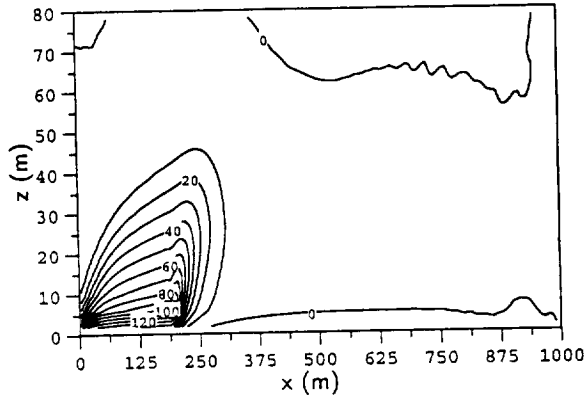
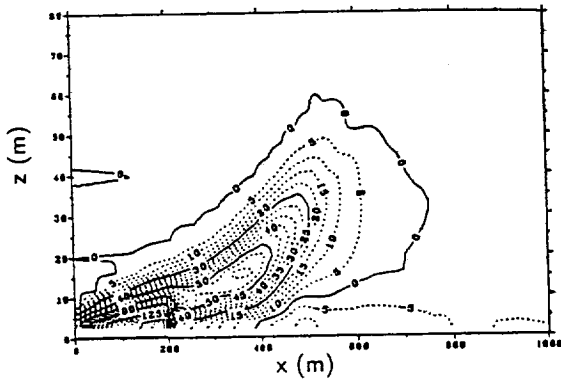


Figure 1: Mean total vertical turbulent temperature flux ( $\text{K m s}^{-1}$ , scaled by  $10^3$ ) for a 200 m lead,  $90^\circ$  wind orientation: GB92 (top), CRM (bottom).

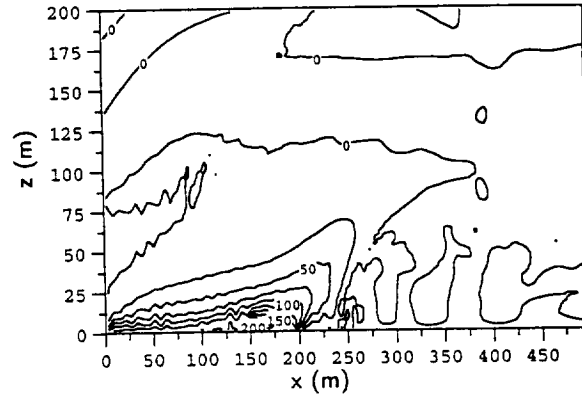
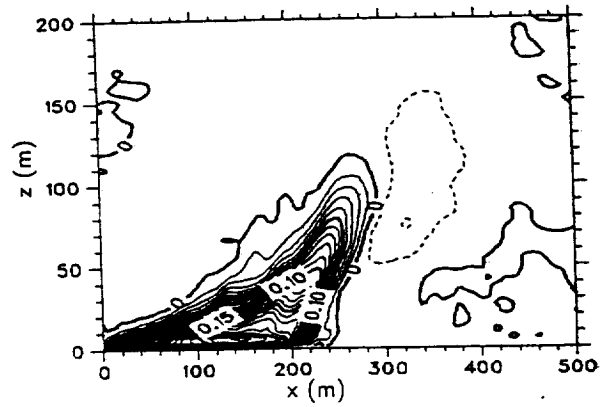


Figure 2: Mean total vertical turbulent temperature flux ( $\text{K m s}^{-1}$ ) for a 200 m lead,  $15^\circ$  wind orientation: G94 (top), CRM (bottom, scaled by  $10^3$ ).

Fig. 2 displays the temperature fluxes obtained when the geostrophic wind is aligned at a  $15^\circ$  angle with respect to the lead. Despite the longer transit time, slightly less than  $P$ , the maximum plume development remains downstream of the lead, much like the  $90^\circ$  case. The resulting plumes do penetrate deeper (to approximately 120 m). Compared with the CRM, however, the LES displays larger values of the temperature flux reaching slightly higher in the atmosphere, but otherwise the resulting plumes are quite similar.

In Fig. 3 the geostrophic wind is parallel to the lead. Even though there is no large-scale cross-wind, frictional turning of the geostrophic forcing near the surface (the Ekman spiral) causes both plumes to be tilted slightly to the left. It is obvious that the lack of an imposed cross-wind allows the plumes to transport heat much higher into the inversion. The magnitude of the fluxes agree quite well between the two simulations, while the CRM allows the plume to penetrate slightly higher than the LES (approximately 175 m vs. 160 m).

#### 4. EFFECTS OF VARYING LEAD WIDTH

Lead width variation can impact the resulting circulations in a number of ways. The primary effect appears to be that by increasing the warm water surface area, more heat is transferred to the atmosphere, which in turn enhances the local circulations. Among the secondary effects is the fact that wider leads have longer transit times for a given wind field, which facilitates plume development. Another secondary effect is that a wider lead, with its enhanced circulation and inflows, will display greater surface heat fluxes. The increased fluxes further intensify the circulations, forming a positive feedback that can amplify substantially the resulting plumes. The lead fraction (ratio of lead surface area to total surface area) also has an impact upon the circulations. An increase in lead fraction expedites the plume's erosion of the inversion, thereby allowing the plumes to attain greater heights.

In Fig. 4, vertical velocities are displayed for three CRM simulations, for 200 m, 400 m, and 800 m wide leads. Because the geostrophic wind is parallel to the leads (to simplify the analysis) and the plumes develop

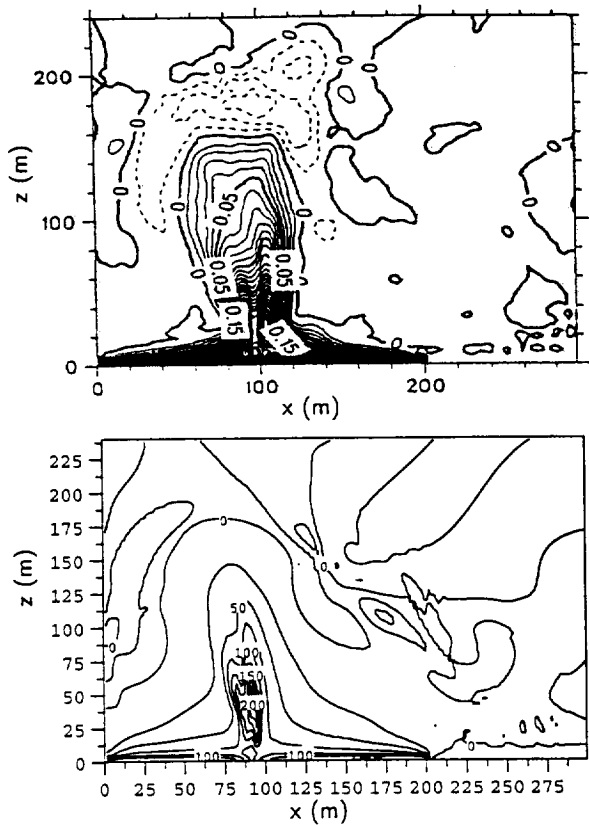


Figure 3: Mean total vertical turbulent temperature flux ( $\text{K m s}^{-1}$ ) for a 200 m lead,  $0^\circ$  wind orientation: G94 (top), CRM (bottom, scaled by  $10^3$ ).

over the leads, the transit time is not a factor. The lead fraction is approximately the same in the three plots, (though substantially different from that used in earlier figures). The difference in the plumes displayed in Fig. 4 is thus mainly a result of the increase in warm water surface area, and thereby an increase in the heat transfer to the atmosphere. As expected, the wider leads result in deeper and more vigorous circulations. The plumes attain depths of approximately 175 m, 200 m, and 300 m for the 200 m, 400 m, and 800 m wide leads, respectively. The maximum vertical velocities increase in a similar fashion.

The surface sensible heat fluxes average approximately  $240 \text{ W m}^{-2}$  over the 200 m lead,  $250 \text{ W m}^{-2}$  over the 400 m lead, and  $270 \text{ W m}^{-2}$  over the 800 m lead. Though these increases are modest and probably do not affect plume development greatly, Fig. 5 displays a case where the surface flux feedback is more substantial. For this case, in a quiescent environment, the average sensible heat flux over a 10 km wide lead is  $422 \text{ W m}^{-2}$  (CRM results). Also shown in Fig. 5 are results from AC95 for a 10 km lead using the same parameters. Note that the plot from AC95 displays their

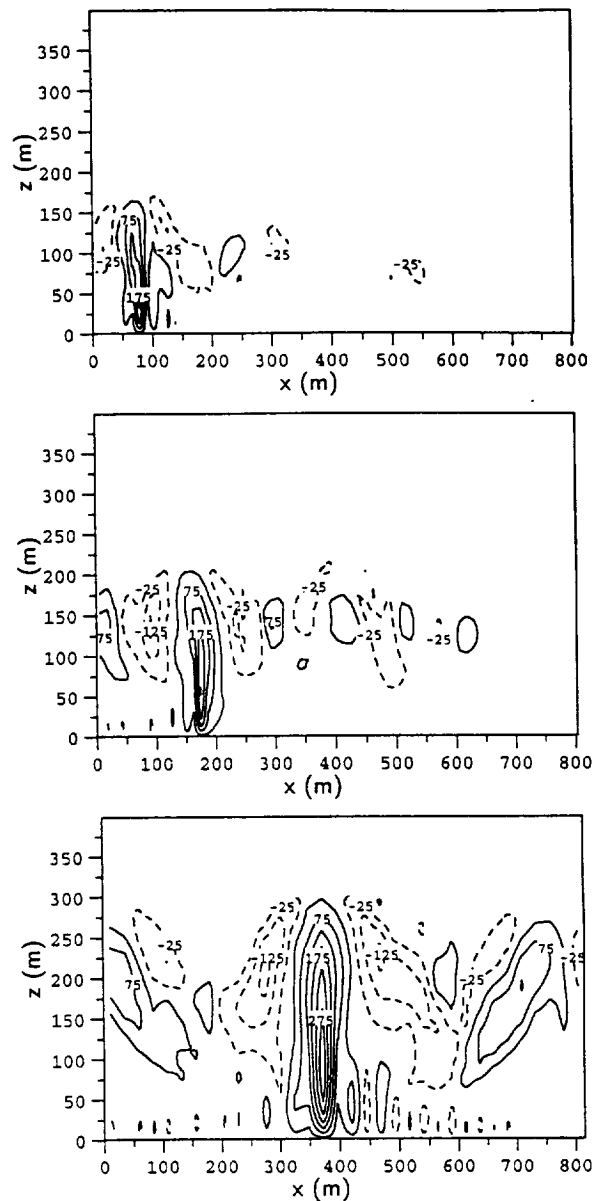


Figure 4: Mean vertical velocity ( $\text{cm s}^{-1}$ ) for  $0^\circ$  wind orientation: 200 m lead (top), 400 m lead (middle), 800 m lead (bottom).

stretched vertical coordinate, and that the units on the axes are in km rather than m.

Fig. 5 compares the vertical velocities obtained after six hours of integration. Note the striking differences between the results of AC95 and the present CRM results, especially plume height. AC95 found that the plume penetrated to an altitude of approximately 2 km, while in the present study the CRM plume height is less than 800 m. Also, after 6 hours, the AC95 plume appeared to still be growing at a substantial rate, while the CRM results indicate slight growth. A possible ex-

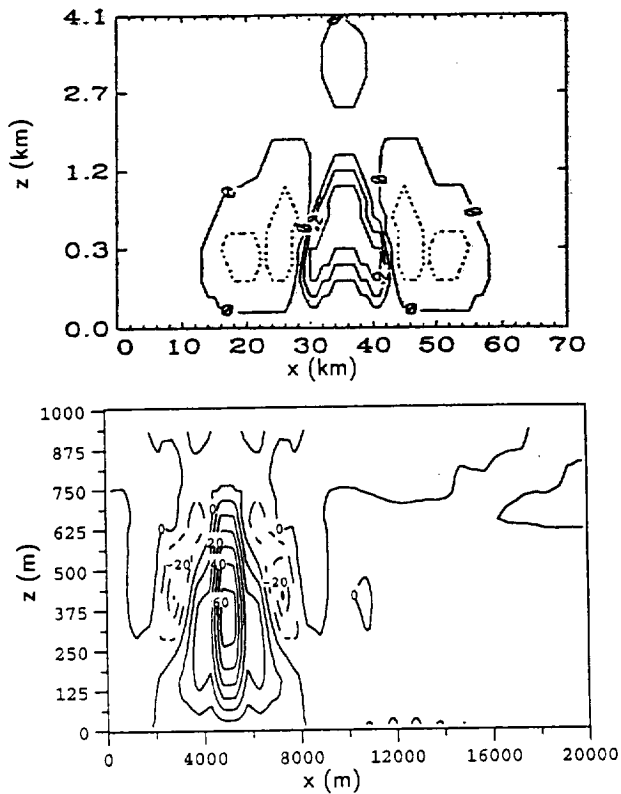


Figure 5: Mean vertical velocity ( $\text{cm s}^{-1}$ , with  $10 \text{ cm s}^{-1}$  contour intervals) for a 10 km lead, no geostrophic wind: AC95 (top), CRM (bottom).

planation for the disparities between these results is the more advanced turbulence closure scheme employed by the CRM.

## 5. COMPARISONS WITH THEORETICAL RESULTS

Additional evidence that the CRM is accurately predicting plume height may be obtained by comparing model results with those from theoretical methods. A similarity solution like those of Emanuel (1994) may be obtained for the case where the large-scale geostrophic wind is parallel to the lead. To eliminate any feedbacks caused by the increased surface flux, the heat flux over the lead is specified at  $250 \text{ W m}^{-2}$ . The top portion of Fig. 6 compares CRM results with those obtained from similarity theory. Although specifying the fluxes, rather than diagnosing them normally, affects the plume circulations, the excellent agreement with theory leads us to believe that we are handling the basic physics of the problem accurately.

Comparisons with theory become more complicated when the geostrophic cross-wind is non-negligible. Fig. 6 also compares the theoretical heights calculated using the dimensional solution given by GB92 with

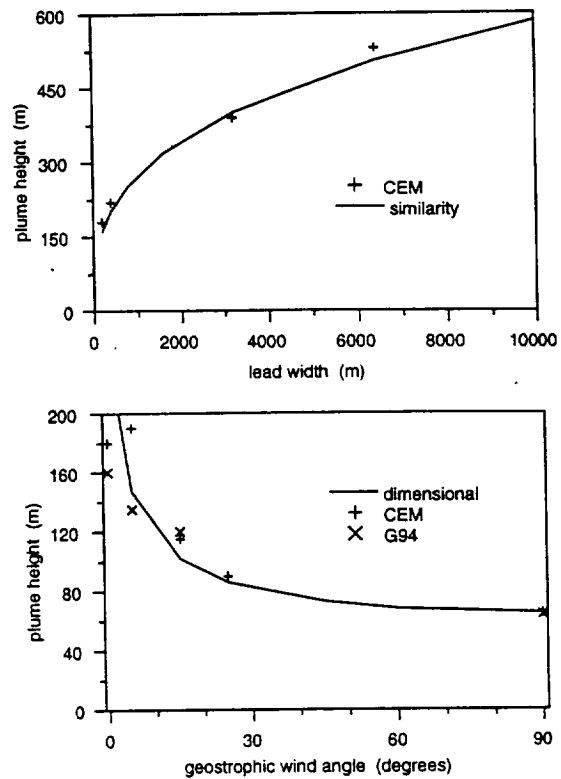


Figure 6: Comparison of simulation derived plume heights with theoretical solutions for cases with specified fluxes and no geostrophic cross-wind (top), and those with natural fluxes and geostrophic cross-wind (bottom).

CRM results for this situation. A 200 m lead with a  $2.5 \text{ m s}^{-1}$  geostrophic wind at varying wind-to-lead orientation is used. The surface sensible heat fluxes are diagnosed, rather than prescribed, and are all approximately  $250 \text{ W m}^{-2}$  (the value used for the dimensional solution). For comparison, the LES results from G94 are included on the plot. The excellent agreement between theory, LES, and CRM results suggests that the plumes are being handled adequately.

## 6. EFFECTS OF ADDITIONAL PHYSICS

For reasons of computational requirements or complexity, many studies have neglected microphysical and radiative processes. For the most part, this is a valid simplification, because at the temperatures and time scales of interest, sensible heating is thought to be the dominant process. Nonetheless, these other processes should also be investigated, especially since the addition of moisture to the Arctic atmosphere is of primary interest. As we are presently interested in the Arctic winter, solar radiation need not be considered.

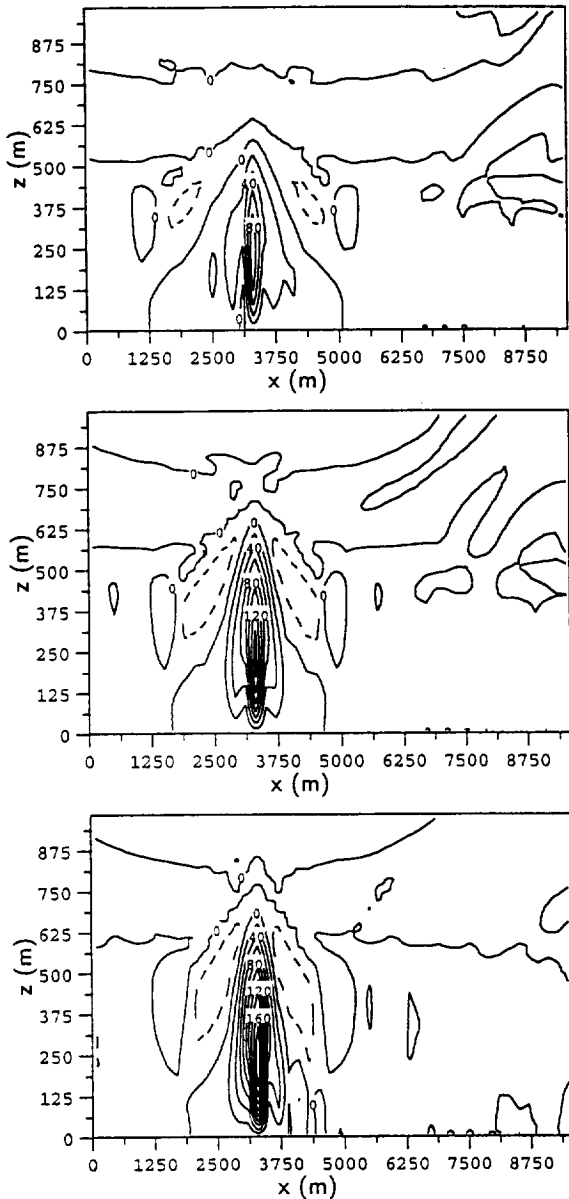


Figure 7: Mean vertical velocity ( $\text{cm s}^{-1}$ ) for a 6400 m lead,  $0^\circ$  wind orientation: no microphysics and no radiation (top), includes microphysics (middle), includes microphysics and radiation (bottom).

Based on the present CRM results, it appears that the addition of microphysical and radiative processes has a greater impact upon the more energetic circulations, such as those associated with wider leads. Fig. 7 displays the results obtained for a 6400 m lead under three configurations. The first is with no additional physics; the second is with the addition of microphysical processes; and the third is with the addition of microphysical and radiative processes. Although the structure of the resulting plumes is not appreciably al-

tered, the depth and maximum vertical velocities do increase. For the first simulation, the plume reaches a depth of about 630 m. The addition of microphysics increases the plume depth by 60 m, and the further addition of radiative processes yields a plume height of 780 m. Thus, the inclusion of the additional physics increases the plume depth by nearly 25%.

The increase in circulation strength is due mainly to two factors. The surface latent heat flux is nearly one third the magnitude of the sensible heat flux. The amount of latent heat that is actually released through condensation depends upon the strength of the circulation and the initial moisture profile. This explains why microphysical processes typically have a greater impact upon larger leads, as their stronger circulations are able to lift the moist air higher, resulting in increased condensation and latent heating. For the simulations described herein, the initial moisture profile is set to 85% RH (with respect to ice). The addition of radiative processes results in a significant warming (through IR flux divergence) of the air directly above the lead. The radiation is also responsible for substantial IR cooling at the top of the plume, but the impact is more limited than caused by the heating, resulting in a net increase of the circulation strength.

#### ACKNOWLEDGMENTS

This research was supported by NSF Grant OPP-9702583 and NASA Grant NAG-1-1718.

#### REFERENCES

- Alam, A., and J. Curry, 1995: Lead-induced atmospheric circulations. *J. Geophys. Res.*, **100**, 4643–4651.
- Emanuel, K. A., 1994: *Atmospheric Convection*. Oxford University Press, 580 pp.
- Glendening, J. W., and S. D. Burk, 1992: Turbulent transport from an Arctic lead: A large-eddy simulation. *Bound. Layer. Meteor.*, **59**, 315–339.
- Glendening, J. W., 1994: Dependence of a plume heat budget upon lateral advection. *J. Atmos. Sci.*, **51**, 3517–3530.
- Krueger, S. K., McLean, G. T., and Q. Fu, 1995: Numerical simulation of the stratus to cumulus transition in the subtropical marine boundary layer: I. Boundary layer structure. *J. Atmos. Sci.*, **52**, 2839–2850.

Steven K. Krueger\* and Shuairan Liu  
University of Utah, Salt Lake City, Utah

Qiang Fu  
Dalhousie University, Halifax, Nova Scotia, Canada

The entrainment rate at the top of the atmospheric boundary layer is affected by many processes, such as radiation, evaporation, and boundary layer circulations. An intercomparison of radiatively driven entrainment and turbulence in a smoke cloud (Bretherton et al. 1997; hereafter B97) investigated an idealized case in which a convective boundary layer filled with radiatively active "smoke" is simulated by several 1D, 2D, and 3D models. Cloud-top cooling rates were chosen to be comparable to those observed in marine stratocumulus, while avoiding evaporative feedbacks on entrainment and turbulence that are also important in liquid water clouds. The radiative cooling rate had a specified dependence on the smoke profile, so that differences between simulations could only be a result of different numerical representations of fluid motion and subgrid-scale turbulence.

We used this case to test the University of Utah 1D turbulent closure model (UU TCM). The UU TCM also participated in a similar, but more complicated, intercomparison of simulations of a stratocumulus-topped boundary layer that motivated the smoke cloud intercomparison (Moeng et al. 1996). The UU TCM is the 1D version of the UU Cloud Resolving Model (Krueger 1988). The UU TCM is based on third-moment turbulence closure, which includes prognostic equations for first moments (including the horizontally averaged potential temperature and smoke mixing ratio), second moments (including the horizontal and vertical velocity variances and the vertical fluxes of sensible heat and smoke), and third moments (including the vertical fluxes of the horizontal and vertical velocity variances).

The initial boundary layer was assumed to be at constant potential temperature and uniformly filled with smoke (with a mixing ratio of 1) over its whole 700 m depth. Above the boundary layer the smoke concentration was set to zero. The standard requirement was that models should use a vertical grid size of 25 m and be run to simulate a period of 3 h.

Fig. 1 shows the 2-3 h average turbulent kinetic energy (TKE) budget for the UKMO 3D high-resolution large-eddy simulation (LES) model and the UU TCM.

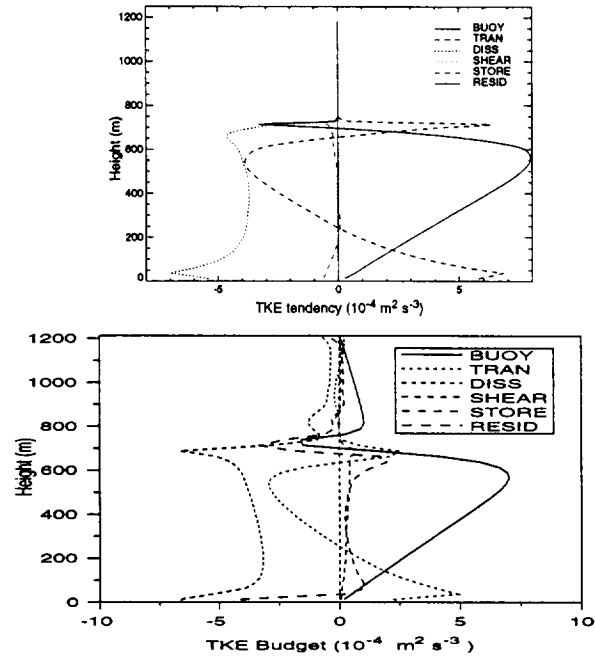


Figure 1: 2-3 h average TKE budget for the UKMO 3D high-resolution model (top; from B97) and the UU TCM (bottom).

The TKE budget for the UU TCM agrees well with that of the LES. The most notable differences occur above the boundary layer, where the UU TCM produces a spurious turbulent layer.

Figs. 2 and 3 show the potential temperature and smoke mixing ratio profiles averaged over 2-3 h for the UU TCM, while Figs. 4 and 5 show the corresponding turbulent flux profiles. When these are compared with the corresponding plots in B97, it is evident that the profiles of potential temperature, smoke, heat flux, and smoke flux from the UU TCM agree well with 3D large-eddy simulations involved in the intercomparison. The only significant differences occur above the boundary layer, where the UU TCM produces spurious fluxes of both heat and smoke.

In B97, results from numerous modeling groups around the world were compared with each other and

\* Corresponding author address: Department of Meteorology, University of Utah, Salt Lake City, UT 84112. E-mail: skrueger@atmos.met.utah.edu

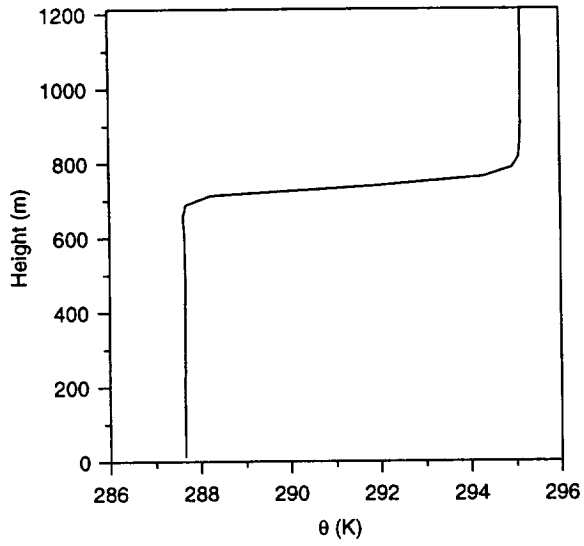


Figure 2: Potential temperature profile averaged over 2-3 h for the UU TCM.

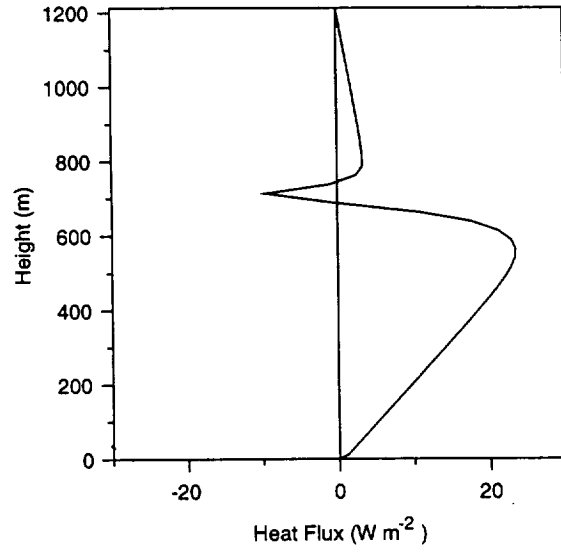


Figure 4: Heat flux profile averaged over 2-3 h for the UU TCM.

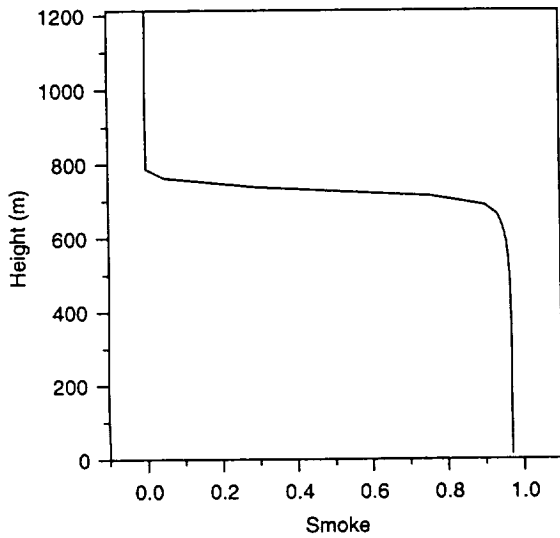


Figure 3: Smoke mixing ratio profile averaged over 2-3 h for the UU TCM.

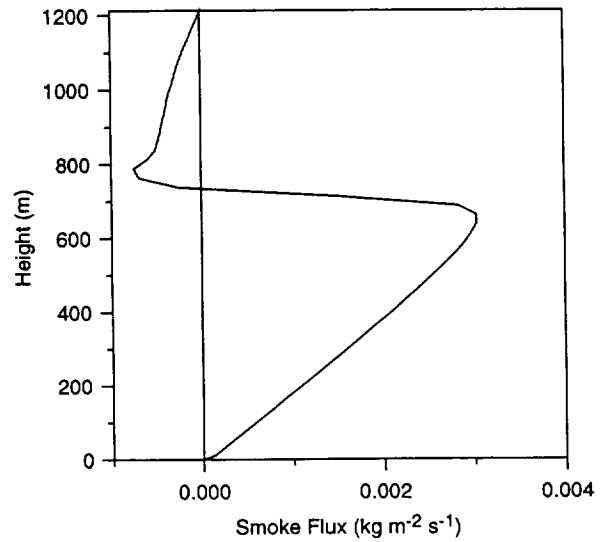


Figure 5: Smoke flux profile averaged over 2-3 h for the UU TCM.

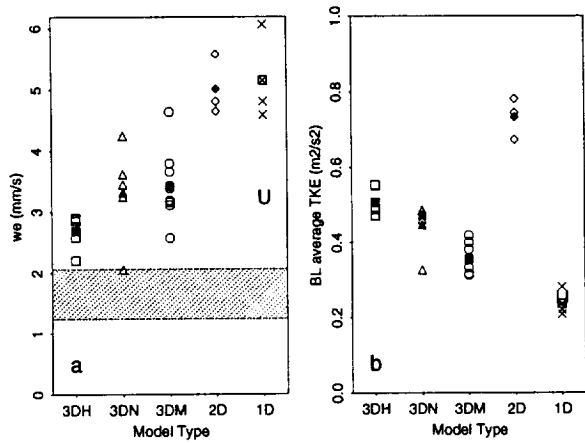


Figure 6: Scatterplot of 2-3 h averages of (a)  $w_e$ , (b)  $TKE_{blav}$ , partitioned by group. Filled symbols (crossed square for 1D) indicate means for each group. "U" shows the result for the UU TCM. Hatched zone in (a) indicates prediction based on laboratory analog. (After B97.)

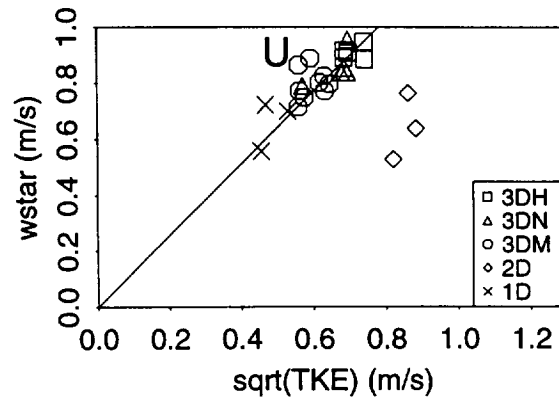


Figure 8: Scatterplot of  $w_*$  vs.  $\sqrt{TKE_{blav}}$  for all models. "U" shows the result for the UU TCM. Best-fit line is derived from the 3DH models. (After B97.)

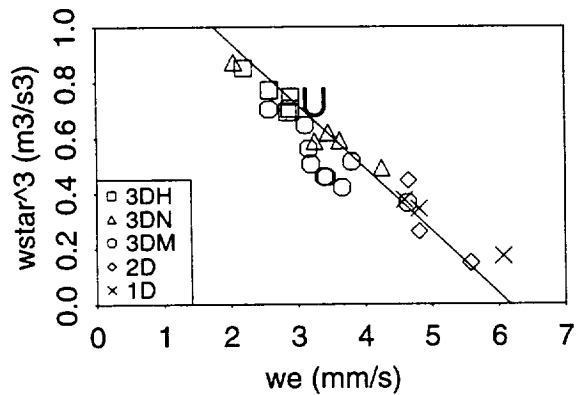


Figure 7: Scatterplot of  $w_*^3$  vs.  $w_e$  for all models. "U" shows the result for the UU TCM. The line is the prediction of (11) in B97. (After B97.)

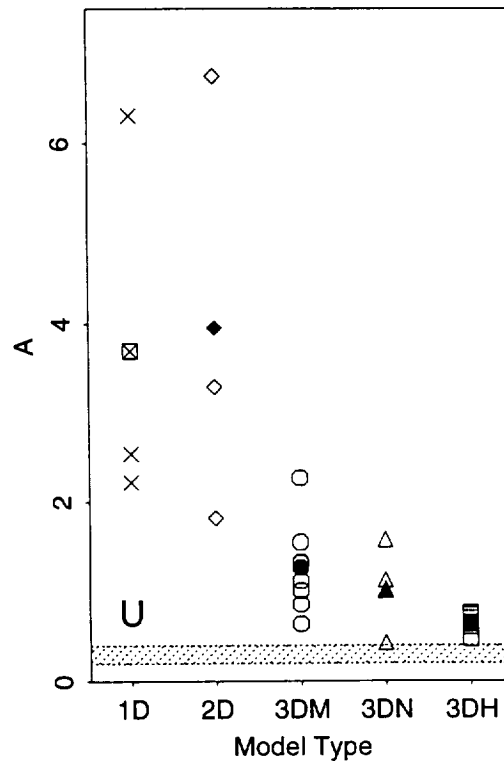


Figure 9: As in Fig. 6a, except for A. (After B97.)

with a previously investigated laboratory analog to the smoke cloud. We will compare the results from the UU TCM to these results.

Fig. 6 is a scatterplot of 2-3 h averages of the entrainment velocity,  $w_e$ , and the TKE averaged over the boundary layer,  $\text{TKE}_{\text{blav}}$ , partitioned by model group: three-dimensional, high resolution (3DH); three-dimensional, standard resolution with non-monotone advection (3DN) or monotone advection (3DM); two-dimensional (2D) and one-dimensional (1D). The symbol "U" shows the result for the UU TCM. The hatched zone in (a) indicates the prediction based on the laboratory analog (see B97 for details). The entrainment velocity for the UU TCM is much lower than that for other 1D models, and is in the same range as that of the 3D standard-resolution models (3DN and 3DM). Whether this is a robust feature of third-moment turbulence closure models, or is an artifact of this particular model, remains to be determined.

Fig. 7 is a scatterplot of  $w_*^3$  vs.  $w_e$  for all models, where  $w_*$  is the convective velocity scale. The line is the prediction of Eq. (11) in B97, which was derived under the assumption that the boundary layer is well-mixed. The point for the UU TCM falls near the theoretical line along with those from the 3D models.

Fig. 8 is a scatterplot of  $w_*$  vs.  $\sqrt{\text{TKE}_{\text{blav}}}$  for all models. The best-fit line is derived from the 3DH models. The point for the UU TCM is above the best-fit line. The reason for this is not understood.

Fig. 9 is a scatterplot of 2-3 h averages of  $A$ , the entrainment efficiency (proportional to  $w_e/w_*^3$ ), partitioned by model group. The hatched zone shows the range suggested by the laboratory experiments. (See B97 for details.) The value for the UU TCM is similar to that of the 3D models.

ACKNOWLEDGMENTS. This research was supported by NASA Grants NAG-1-1718 and NAG-1-2048.

## REFERENCES

- Bretherton, C. S., M. K. MacVean, P. Bechtold, A. Chlond, W. R. Cotton, J. Cuxart, H. Cuijpers, M. Khairoutdinov, B. Kosovic, D. Lewellen, C.-H. Moeng, P. Siebesma, B. Stevens, D. E. Stevens, I. Sykes, and M. C. Wyant, 1997: An intercomparison of radiatively-driven entrainment and turbulence in a smoke cloud, as simulated by different numerical models. *Quart. J. R. Meteor. Soc.*, submitted 5/97.
- Krueger, S.K., 1988: Numerical simulation of tropical cumulus clouds and their interaction with the subcloud layer. *J. Atmos. Sci.*, **45**, 2221–2250.
- Moeng, C.-H., W.R. Cotton, C. Bretherton, A. Chlond, M. Khairoutdinov, S. Krueger, W.S. Lewellen, M.K. McVean, J.R.M. Pasquier, H.A. Rand, A.P. Siebesma, R.I. Sykes, and B. Stevens, 1996: Simulation of a stratocumulus-topped PBL: Intercomparison of different numerical codes. *Bull. Amer. Meteor. Soc.*, **77**, 216–278.

Steven K. Krueger\* and Shuairan Liu  
University of Utah, Salt Lake City, Utah

Qiang Fu  
Dalhousie University, Halifax, Nova Scotia, Canada

Despite the recognition that Arctic stratus clouds (ASC) have a significant effect on the surface energy budget of the Arctic, and thereby on the sea ice thickness, the formation mechanism(s) of these clouds are still uncertain. This is largely due to the obvious logistical difficulties of making extensive observations in the Arctic. However, limited observations have been made, including during the Arctic Stratus Experiment in the Beaufort Sea during June 1980. These and other observations of the structure of the summertime arctic boundary layer were summarized by Curry et al. (1988). They noted that ASC differ in several aspects from marine subtropical stratus clouds. ASC often occur in multiple layers. The lowest layer may rest on the surface. The upper cloud layer or layers are decoupled from the stable surface layer, thus their source of water vapor does not appear to be the surface.

The formation of ASC was studied by Curry and Herman (1985) using large-scale budgets derived from operational analyses. They concluded that ASC form as relatively warm and moist air flows into the Arctic from lower latitudes and is cooled radiatively and by contact with the colder surface of the sea ice and ocean.

Three mechanisms have been proposed to explain the layering of ASC. The 1D turbulence closure-radiative transfer model results of Herman and Goody (1976) support the idea that solar absorption warms the interior of a surface-based cloud and thereby forms a clear layer between two cloudy layers. Tsay and Jayaweera (1984) proposed that the upper cloud layer is formed by very weak ascent or entrainment, while the surface cloud layer is an advective fog. McInnes and Curry (1995) suggested that the upper cloud layer is maintained by cloud-top radiative cooling, while the lower cloud layer is formed by radiative cooling at the base of the upper mixed layer.

Modeling studies that used 1D second-moment turbulence models have reproduced many aspects of the structure of the summertime Arctic boundary layer (Finger and Wendling 1990; McInnes and Curry 1995).

\* Corresponding author address: Department of Meteorology, University of Utah, Salt Lake City, UT 84112. E-mail: skrueger@atmos.met.utah.edu

In this preprint, we present some preliminary results on the sensitivity of the formation and structure of simulated Arctic summertime boundary-layer clouds to large-scale vertical velocity and drizzle using the University of Utah 1D turbulent closure model (UU TCM). The UU TCM includes third-moment turbulence closure, a drizzle parameterization, and an interactive radiative transfer scheme. The UU TCM is the 1D version of the UU Cloud Resolving Model (Krueger 1988).

The UU TCM has been tested against 3D large-eddy simulation models in two recent model intercomparisons that involved simulations of cloud-topped boundary layers (Moeng et al. 1996; Krueger et al. 1999). In both intercomparisons, the UU TCM's boundary layer vertical structure and entrainment rate were nearly the same as those obtained from the large-eddy simulation models.

Here we present the results of two sets of integrations. In one set (Cases B, W1, W2, and W3) only the large-scale vertical velocity  $\bar{w}$  is varied, while in the second set (Cases Cases B, D1, and D2), only the drizzle parameterization is changed. Case B is the baseline case against which the others are compared. Table 1 lists the cases.

The drizzle parameterization labeled "Chen" in Table 1 follows Chen (1996) and Wang and Wang (1994). The parameters we used lead to an autoconversion threshold of  $0.38 \text{ g kg}^{-1}$ . We chose to use an autoconversion rate of  $0.0002 \text{ s}^{-1}$  which corresponds to Wang and Wang's "light drizzle" case. The parameterization labeled "Kessler" uses Kessler's warm rain microphysics as described in Krueger (1988) except that the autoconversion threshold is reduced to  $0.3 \text{ g kg}^{-1}$ . The autoconversion rate remains unchanged at  $0.001 \text{ s}^{-1}$ .

The initial conditions for our integrations are based on the observations of an Arctic summertime boundary layer obtained on June 28, 1980, during the Arctic Stratus Experiment (McInnes and Curry 1995). In the integrations, the effective radius of the cloud droplets is 7 microns, the surface albedo is 0.55, the solar zenith angle is 74 degrees, and the vertical grid size is 25 m. Each case was run for 10 hours of physical time.

Fig. 1 presents time-height plots of cloud water mix-

Table 1: List of cases.

Case	$\bar{w}$ (mm s <sup>-1</sup> ) at $z = 1000$ m	Drizzle Parameterization
B	0.0	Chen
W1	-0.2	Chen
W2	-0.5	Chen
W3	-4.0	Chen
D1	0.0	Kessler
D2	0.0	(none)

ing ratio for Cases B, W1, W2, and W3. The baseline case, under conditions of no large-scale vertical motion, contains two layers of clouds: a stable fog layer near the surface and a stratus cloud in an elevated mixed layer. The top of the upper cloud layer ascends slowly due to entrainment. Cases W1, W2, and W3 show that large-scale subsidence delays the formation of the upper cloud layer, and increases the liquid water content of the fog layer.

Fig. 2 includes time-height plots of cloud water mixing ratio for Cases D1 and D2. These should be compared to the baseline case plot in Fig. 1. The main impact of changing the drizzle parameterization from Chen to Kessler is to slightly reduce the peak cloud water mixing ratios in the upper cloud layer, while neglecting drizzle slightly increases them. The impact of changing or not including the drizzle parameterization is considerably greater in the fog layer due its larger peak cloud water mixing ratios. It should be noted that in the cases with drizzle, the downward turbulent flux of water at the surface is comparable to the drizzle flux.

ACKNOWLEDGMENTS. This research was supported by NASA Grants NAG-1-1718 and NAG-1-2048.

## REFERENCES

- Chen, A., 1996: Studies of stratocumulus cloud, drizzle, and aerosol interaction. Masters thesis, Department of Atmospheric Science, Colorado State University, Fort Collins, 101 pp.
- Curry, J.A., and G.F. Herman, 1985: Relationships between large-scale heat and moisture budgets and the occurrence of Arctic stratus clouds *Mon. Wea. Rev.*, **113**, 1441-1457.
- Curry, J.A., E.E. Ebert, and G.F. Herman, 1988: Mean and turbulence structure of the summertime Arctic cloudy boundary layer. *Quart. J. Roy. Met. Soc.*, **114**, 715-746.
- Finger, J.E., and P. Wendling, 1990: Turbulence structure of Arctic stratus clouds derived from measurements and calculations. *J. Atmos. Sci.*, **47**, 1351-1373.
- Herman, G., and R. Goody, 1976: Formation and persistence of summertime Arctic stratus clouds. *J. Atmos. Sci.*, **33**, 1537-1553.
- Krueger, S.K., 1988: Numerical simulation of tropical cumulus clouds and their interaction with the subcloud layer. *J. Atmos. Sci.*, **45**, 2221-2250.
- Krueger, S. K., S. Liu, and Q. Fu, 1999: Radiatively driven entrainment and turbulence in a smoke cloud. *Preprints, 13th Symposium on Boundary Layers and Turbulence*, Dallas TX, Amer. Meteor. Soc., (in press).
- McInnes, K. and J.A. Curry, 1995: Modelling the mean and turbulent structure of the arctic summertime cloudy boundary layer. *Bound. Layer Meteor.*, **73**, 125-143.
- Moeng, C.-H., W.R. Cotton, C. Bretherton, A. Chlond, M. Khairoutdinov, S. Krueger, W.S. Lewellen, M.K. McVean, J.R.M. Pasquier, H.A. Rand, A.P. Siebesma, R.I. Sykes, and B. Stevens, 1996: Simulation of a stratocumulus-topped PBL: Intercomparison of different numerical codes. *Bull. Amer. Meteor. Soc.*, **77**, 216-278.
- Tsay, S.-C., and K. Jayaweera, 1984: Physical characteristics of Arctic stratus clouds. *J. Climate Appl. Meteor.*, **23**, 584-596.
- Wang, S., and Q. Wang, 1994: Roles of drizzle in a one-dimensional third-order turbulence closure model of the nocturnal stratus-topped marine boundary layer. *J. Atmos. Sci.*, **51**, 1559-1576.

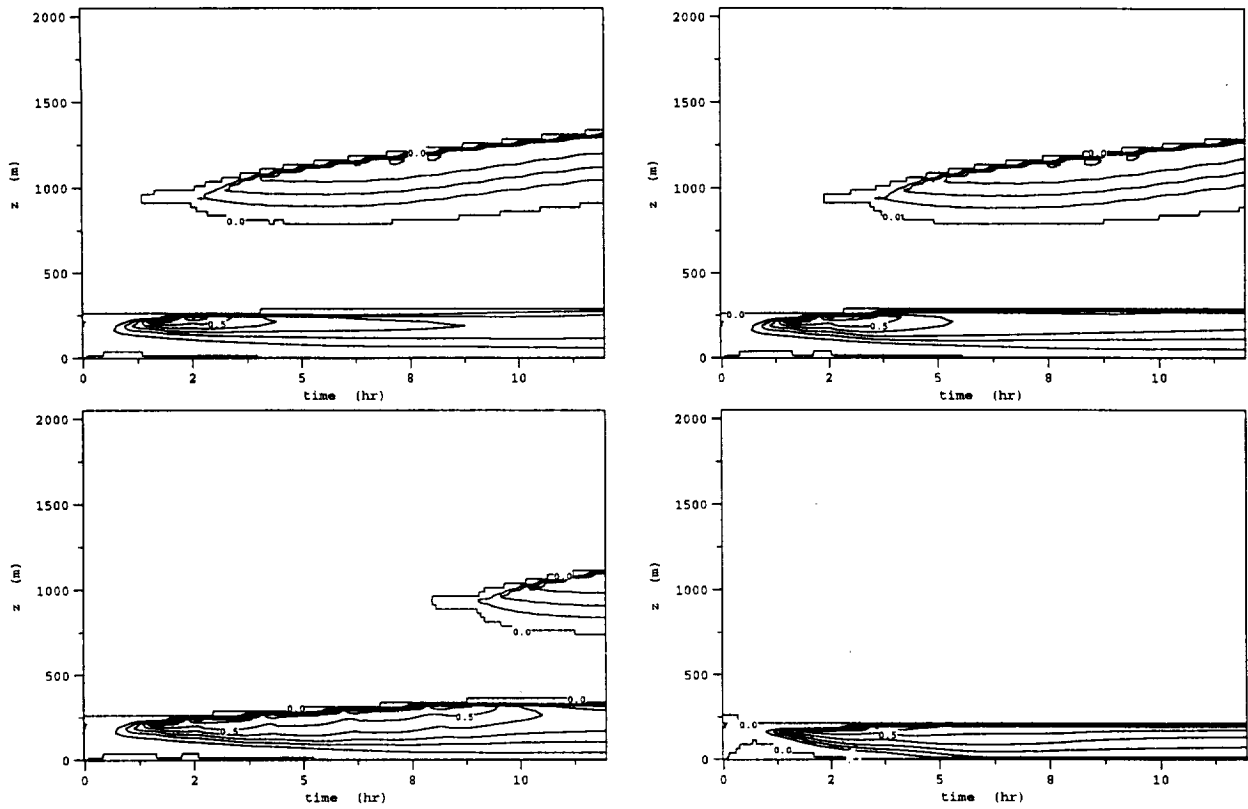


Figure 1: Time-height plots of cloud water mixing ratio ( $\text{g kg}^{-1}$ ) for Cases B (upper left), W1 (upper right), W2 (lower left), and W3 (lower right).

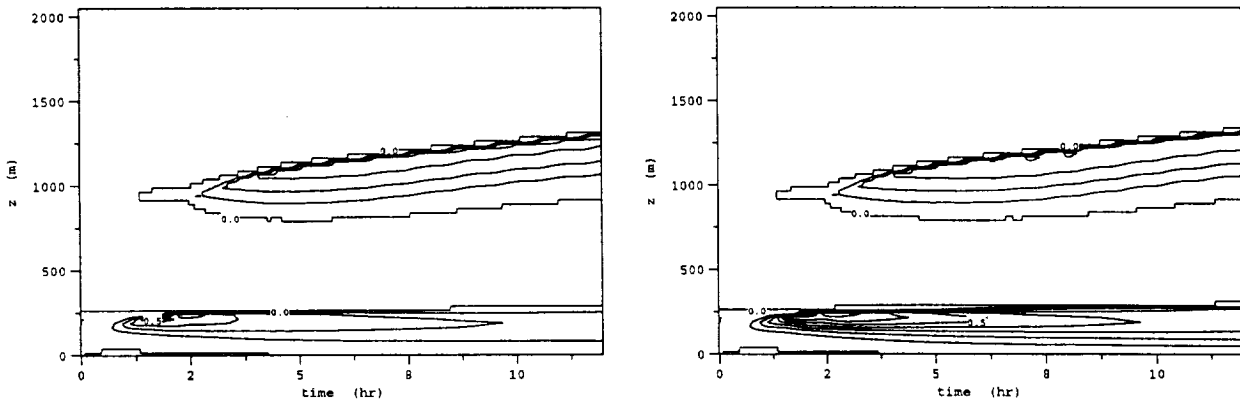


Figure 2: Time-height plots of cloud water mixing ratio ( $\text{g kg}^{-1}$ ) for Cases D1 (left) and D2 (right).